From Bird Flocks to Wireless Sensor Networks: A Congestion Control Approach

Pavlos Antoniou, Andreas Pitsillides, Tim Blackwell, Andries Engelbrecht, and Loizos Michael

Abstract

This study shows that the flocking behavior of birds can, in fact, support a robust and self-adaptive congestion control protocol in the context of wireless sensor networks (WSNs). The proposed approach adopts a swarm intelligence paradigm inspired by the collective behavior of bird flocks having global self-* properties and emergent behavior achieved collectively without explicitly programming these properties into individual nodes. The proposed approach aims at being simple to implement at the individual node, involving minimal information exchange.

The main idea is to 'guide' packets (birds) to form flocks and flow towards the sink (global attractor), whilst trying to avoid congestion regions (obstacles). The direction of motion of a packet flock is influenced by repulsion and attraction forces between packets, as well as the field of view (FoV) and the artificial magnetic field in the direction of the artificial magnetic pole (sink).

Two different models of the flock-based congestion control (Flock-CC) approach were proposed. Both models are presented in this report. The two models have some important differences. The first model, presented in [1], [2], and [3], is more complex and involves three tunable parameters. The second model, mimics more faithfully the bird flocking paradigm, as presented by Couzin at al. [4] and it is simple since it involves only one tunable parameter. Hence easier to tune and thereafter deploy. Even though is simpler, the second model maintains comparably good performance characteristics to the first model. The development of the second model passed through several stages over which different options for (a) repulsion and attraction forces, (b) FoV aperture, and (c) magnetic field imposition were progressively added to the model.

Performance evaluations focused on performing parameter setting and on presenting the effectiveness and efficiency of each Flock-CC model. Both models were found to achieve graceful performance degradation in terms of packet delivery ratio, packet loss, delay and energy tax under low, medium and high traffic loads. In addition, these models were shown to be robust against failing nodes and to outperform typical conventional approaches.

Index Terms

Wireless Sensor Networks (WSNs), Congestion Control (CC), Bird Flocking Behavior.

I. Introduction

OVER the last few years, there has been an unprecedented research interest in the area of autonomous networked systems with emphasis on WSNs [5]. WSNs have been deployed for several mission-critical tasks (e.g. as platforms for health monitoring, process control, environmental observation, battlefield surveillance), and are expected to operate unattended for extended periods of time. Typically, WSNs comprise of small (and often cheap), cooperative devices (nodes) which may be (severely) constrained in terms of computation capability, memory space, communication bandwidth and energy supply. In the context of WSNs, autonomous nodes may interact (a) with the environment so as to sense or control physical parameters, and (b) with each other in order to exchange information or forward data towards one or more sink nodes. This mass of interactions, in conjunction with variable wireless network conditions, may result in unpredictable behavior in terms of traffic load variations and link capacity fluctuations. The network condition is worsened due to topology changes driven by node failures, mobility, or intentional misbehavior. These stressful situations are likely to occur in WSN environments, thus increasing their susceptibility to congestion.

The problem of congestion in WSNs is getting increasingly complex. This is not due to the problem's definition. That mostly stays the same as in other network types (wired or wireless). On the other hand, two new considerations are emerging: the *size of the problem changes*, the *resources to solve the problem are limited*. The former consideration is mostly encountered in large scale WSNs consisting of several thousands of sensor nodes, while the latter issue is an intrinsic characteristic of WSNs. In addition, the convergent (many-to-one) nature of traffic, especially in single-sink WSNs, necessitates completely different ways of tackling congestion than in traditional end-to-end strategies.

A centralized approach cannot be applied since it provokes several serious drawbacks. Firstly, it leads to excessive communication load in the network which rapidly depletes the batteries. Secondly, centralized decision making for congestion control results in slow reaction to changes in network and traffic conditions. Thirdly, it does not take advantage of the in-network processing capability of sensor networks which permits simple processing and decision-making by individual nodes. Finally, in the event of communication failure, the entire system becomes inoperational.

P. Antoniou and A. Pitsillides are with the Department of Computer Science, University of Cyprus, Cyprus, e-mail: paul.antoniou@cs.ucy.ac.cy, andreas.pitsillides@cs.ucy.ac.cy

L. Michael is with Open University of Cyprus, Cyprus, e-mail: loizos.michael@ouc.ac.cy

T. Blackwell is with the Department of Computing, Goldsmiths College, University of London, UK, e-mail: tim.blackwell@gold.ac.uk

A. Engelbrecht is with the Department of Computer Science, University of Pretoria, South Africa, e-mail: engel@cs.up.ac.za

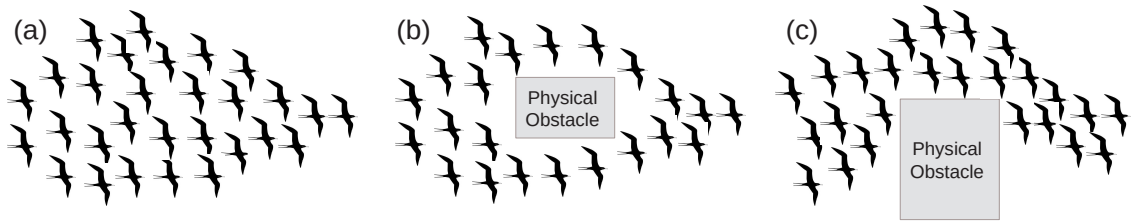

Fig. 1. The obstacle avoidance behavior of bird flocks: (a) A flock of (migrating) birds moves through an obstacle-free environment (towards a magnetic pole); (b) an obstacle 'forces' the flock to split into 2 subflocks; (c) the obstacle extends further on one side and the flock is reformed along the path bypassing the obstacle on the other side.

The limited and unpredictable nature of WSNs necessitates *decentralized, robust, self-adaptive*, and *scalable* mechanisms which are vital to the mission of dependable WSNs. Novel approaches should be *simple* to implement at individual node level with *minimal exchange of information*.

Natural designs are much more sophisticated than man-made designs with inherent powerful characteristics. Natural systems usually exhibit remarkable survivability and robustness to external stimuli and internal perturbations or loss of units, as well as excellent scaling properties. Adaptation is one of the major strengths bio-systems as they must respond to addition or removal of members, as well as to sudden changes in the environment.

WSNs, in many ways, can be likened to social groups found in natural (e.g. bird flocks, ant colonies) attempting to accomplish their tasks collectively (by simple neighbor-to-neighbor interactions), in a decentralized manner, and in the absence of (external) central supervision. This study intends to explore what can be learned from the behavioral tendencies of natural systems for designing robust network control techniques. Drawing inspiration from the collective behavior of social groups, local behavior can be dictated easier and an emergent global behavior of minimum congestion and direction of information flow to the sink can be determined. In this way, self-* properties, e.g. self-organization and self-adaptation, are not implemented explicitly into individual devices or nodes, but emerge as a result of the design of the nature-inspired CC model.

This study aims to provide congestion avoidance by mimicking the *obstacle avoidance behavior of bird flocks* shown in Fig. 1. In the proposed Flock-based Congestion Control (Flock-CC) approach, packets are modeled as birds flying over a topological space, e.g. a sensor network. The main idea is to 'guide' packets to form flocks and flow towards a global attractor (artificial magnetic pole - sink), whilst trying to avoid obstacles (failing nodes and congested regions). Inspiration is drawn by: (a) the repulsive and attractive interactions among closely located individuals proposed by Couzin et al. [4], (b) the orientational movement of migrating birds towards a global attractor (poles or equator), and (c) the limited visual perception (field of view) of individuals within the flock.

Initial attempts towards developing the Flock-CC approach are described in [1], [2], and [3], while are summarized in this report. The new model passed through several design stages which are also presented in the report. The two models have some important differences. Specifically, the new version mimics more faithfully the bird flocking paradigm, as presented by Couzin at al. [4]. Also the new version is simpler, involving only one tunable parameter instead of three (hence easier to tune and thereafter deploy), while it maintains comparably good performance characteristics.

Both Flock-CC models primarily target real-time event-based sensor networks used, for example, in process control and disaster recovery missions. In event-based sensor networks, packet bursts can be dynamically and randomly initiated at any sensor node within the network which is expected to report to the sink once the occurrence of a given event has been detected.

The rest of this paper is organized as follows. Section II introduces the novel paradigm of Swarm Intelligence with emphasis

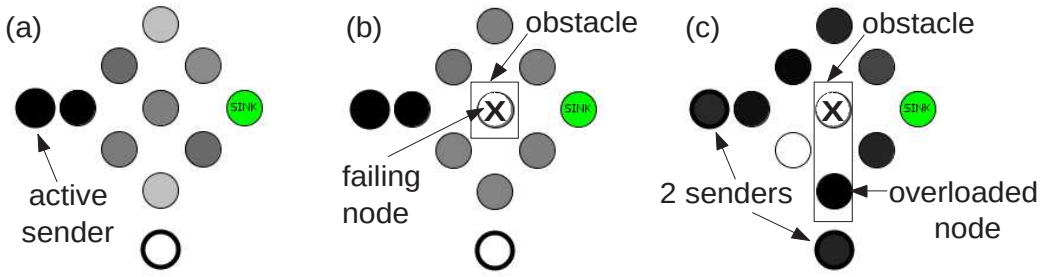

Fig. 2. The obstacle avoidance behavior of packet flocks. Color intensity indicates the intensity of packets visiting within the given 1-second time slot. (a) A flock of packets moves through an obstacle-free environment towards the sink; (b) an obstacle (failing node) 'forces' the flock to split into 2 subflocks; (c) after the activation of the second sender, the obstacle is supplemented by an overloaded node which causes the packet flock coming from the back of the network to follow a less congested path to the sink.

on the flocking behavior of birds. Section III deals with the concept of the flock-based approach, focusing on the two models. In Section IV performance evaluation results for both models are presented and analyzed. Section V draws conclusions and proposes areas of future work.

II. Swarm intelligence and the flocking behavior of birds

This study draws inspiration from nature, which has been very successful in effectively solving similar types of complex problems. Social groups found in nature (e.g. ant colonies, bird flocks, etc.) carry out their tasks collectively in order to contribute to a common goal. Even though individuals coordinate to accomplish a given global mission in a complex world (e.g. foraging, migration, nest building, defence against predators, etc.), an individual has only local perception of the surrounding environment and exhibits specific behavioral tendencies which are governed by a few simple rules.

Recently, nature-inspired computing has been fueled by the emergence of a novel computational paradigm, the so-called Swarm Intelligence (SI) paradigm [6], [7]. SI techniques, motivated by the collective behavior of social insect societies living in decentralized, self-organizing, and adapting environments, reportedly provide a promising basis for computing environments that need to exhibit these characteristics. Research in SI has provided computer scientists with powerful methods for designing distributed control and optimization algorithms. These methods are applied successfully to a variety of scientific and engineering problems [8]. In addition to achieving good performance on a wide spectrum of 'static' problems, swarm-based algorithms tend to exhibit a high degree of flexibility and robustness in dynamic environments [8].

Currently, two of the most successful SI classes of algorithms are Ant Colony Optimization (ACO) and Particle Swarm Optimization (PSO). The research framework behind the majority of network-oriented studies involving self-propelled particles was fueled by the ACO theory proposed by Dorigo et. al [9]. Driven by the collective behavior of ants in finding paths from the colony to food, many researchers [10], [11] tried to solve the problem of routing. In ACO, artificial ants build solutions by moving on the problem graph and, by mimicking real ants, deposit artificial pheromone on the graph in such a way that future artificial ants can build better solutions. The optimal solution can be derived from previously (over suboptimal paths) transmitted messages. The work of Di Caro [10] incorporates congestion awareness in an end-to-end manner (AntHocNet), whereas [11] tries to optimize energy, congestion and load balancing parameters along with providing efficient routing in ad-hoc networks. PSO can be used to tackle specific network-oriented problems like deployment and energy efficiency. Shih [12] implemented a PSO-based clustering algorithm to reduce the traffic load using data aggregation or compression and improve the system's lifetime. Results show that nature-inspired techniques outperform conventional routing algorithms. According to [13], AntHocNet outperforms AODV in terms of delivery ratio, end-to-end delay and jitter. An important observation is that the advantage of AntHocNet over AODV grew for larger networks, especially in terms of overhead, suggesting that AntHocNet is more scalable than AODV. The problem of congestion in decentralized networks is partly addressed using SI techniques, but mostly in the context of ad-hoc networks. However, it has to be noted that ad-hoc and sensor networks have some fundamental differences (see [5] for a detailed explanation) something which drives the necessity for novel CC strategies in the context of sensor networks, on which this study focuses.

The two Flock-CC models involves reference to artificial bird flocks consisting of individuals with the same behavioral model (homogeneity) but with finite range of view (perception) which interact with each other as well as with the environment. The design of the interactions in packet groups is influenced by the study of artificial flocks such as the 'boid' animations of Reynolds [14] and the bio-swarm model of Couzin et al. [4]. The behavior of each individual is influenced by other individuals within its neighborhood.

Both Flock-CC models appear two differences compared to the Couzin's model. The bio-swarm model of Couzin was formulated on the metrical (continuous three-dimensional) space, whereas the Flock-CC model is applied on a two dimensional topological (discrete) space defined by the graph of nodes. In addition, in the Couzin's model (as well as in the Reynolds' model) individuals form flocks and move constantly in a given finite space without any final destination. On the other hand, in Flock-CC, packets are expected to form flocks and move towards a global target which is the sink. The latter Flock-CC characteristic necessitates the existence of an attraction filed towards the sink.

Below, the basic elements of the bird flocking behavior are presented.

A. Repulsion and attraction zones and forces in bird flocks

The Couzin's study [4] investigates how physical and/or motivational differences among individuals may influence the spatial positions of individuals within animal aggregations. The authors abstract animal behavior by placing three concentric behavioral zones around individuals: the rule of cohesion applies in the outer zone (Zone of Attraction, ZoA), alignment applies in a middle zone (Zone of Orientation, ZoO) and at short distances the rule of separation dominates (Zone of Repulsion, ZoR). These zones are spherical, except for a volume behind the individual within which neighbors are undetectable. The notion of the field of view is explained in the next section.

ZoR has the highest priority in the model. If at any time, t, more than one bird resides in the ZoR, the individual bird in the center responds by moving away from the neighbors within this zone. If there is no neighbor within the ZoR, the bird

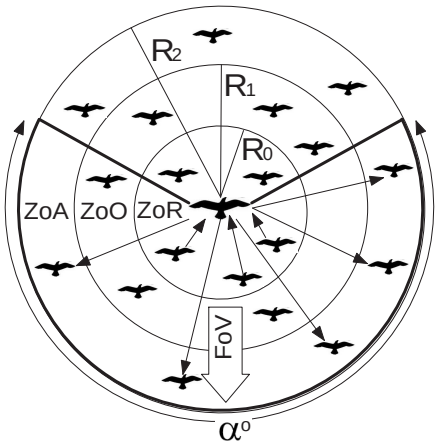

Fig. 3. Representation of the area around a bird placed in the center: ZoR =zone of repulsion, ZoO =zone of orientation, ZoA =zone of attraction. The possible 'blind area' behind an individual is also shown. The aperture of the field of view is α degrees.

responds to others within the ZoO and ZoA. Within the ZoO, the birds align with their neighbors and within the ZoA, the birds move towards each other. Birds cannot see too far, thus there is no interaction with neighbors located outside the ZoA.

The collective flocking behavior of birds, is considered an emergent behavior arising from a few *simple behavioral rules* that are followed by individuals, such as:

1) repel from neighbors (if too close, i.e. within the ZoR) to avoid collisions,
2) attract to neighbors (if apart, i.e. within the ZoA) to maintain coherence among the members of a flock,
3) match velocity (speed and direction) with neighbors (within the ZoO), and
4) introduce a randomness that allows for exploration.

These behavioral rules govern individual-level interactions which collectively result in the emergence of group-level transitions.

B. Birds vision and the field of view

As discussed in the previous paragraph, the motion of each bird is only influenced by its nearest flock mates. Therefore, vision is the most important sense for birds. *The field of view (FoV) determines the extent of the observable world that is seen by each bird at any given moment*. Depending on the placement of the eyes, different animals have different fields of view. Some birds have a 360^o degree overall FoV.

As shown in Fig. 4, the range of visual abilities is not uniform across a field of view, and varies from animal to animal [1].

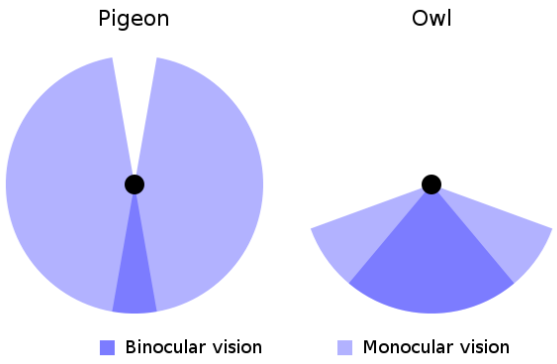

Fig. 4. Fields of view for an owl and a pigeon.

The FoV is modeled in Couzin's study. Fig. 3 shows the 'blind volume' behind the individual. This 'blind volume' is defined as a cone with interior angle $(360 - \alpha)^o$, where α is defined as the FoV of the individual placed in the center. An individual with $\alpha = 360^o$ can respond to others in any direction within the behavioral zones.

[1]The type of vision in which each eye is used separately is called monocular vision. The vision that occurs when the field of vision from each eye overlaps is called binocular vision, and it is quite important for depth perception. Monocular vision refers to the area seen with one eye.

C. Magnetic fields and birds orientation

The aforementioned behavioral rules and the presence of the field of view do not imply that a bird flock will establish a flight path towards a specific attractor. The notion *orientation and attractiveness to a global attractor* can be extracted from the orientational movement of migratory birds. In accordance to [15], migrating birds use the magnetic field for direction finding, either towards magnetic poles (polewards, northern or southern) or the magnetic equator (equatorwards).

It is a biological fact that migrating birds can take advantage of the environment for their movements. Migrating birds can sense the Earth's magnetic field and orientate themselves with the ease of a compass needle. This ability is a massive boon for these birds, keeping frequent flyers on the straight and narrow. The use of magnetic information in bird orientation was discussed in the past, when von Middendorff [16] (1859) proposed what someone, in modern terms, would call a 'magnetic compass', and Viguier [17] (1882) suggested that displaced pigeons use total magnetic intensity and inclination to determine their home direction. In accordance to [15], migrating birds use the magnetic field (Fig. 5) for direction finding, either towards magnetic poles (polewards, northern or southern) or the magnetic equator (equatorwards).

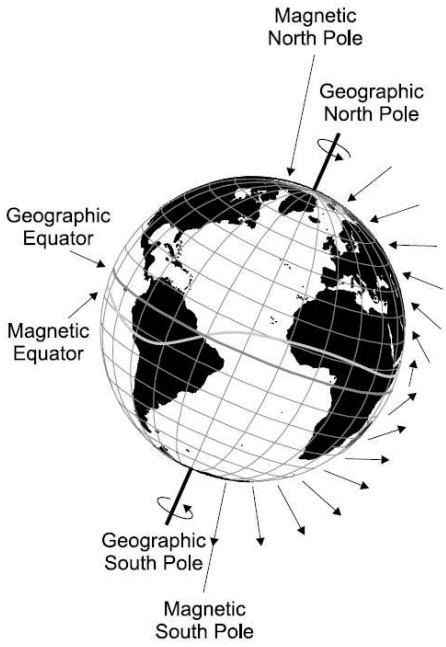

Fig. 5. Schematic drawing of the Earths magnetic field (redrawn from Wiltschko and Wiltschko [18]). The arrows show the course of the magnetic field lines and their length is drawn relative to the magnetic field intensity at different latitudes. The magnetic field intensity is strongest at the magnetic poles (about 68 μT) and weakest at the magnetic equator (about $23\mu T$). The steepness of the magnetic field lines relative to the surface of the Earth shows the angle of inclination, which is maximal at the magnetic poles ($\pm 90^o$) and minimal (0^o) at the magnetic equator.

In addition, the findings summarized in another paper [18], clearly show that the geomagnetic field provides important orientational information[2].

III. Flock-based congestion control (Flock-CC)

A. The concept

A WSN is viewed as a virtual ecosystem, where multiple packets are generated at source nodes and must be directed towards a dedicated sink node. The main idea behind both Flock-CC models is to *'guide' packets to form groups or flocks, and flow towards a global attractor (sink), whilst trying to avoid obstacles (congestion regions)* as illustrated in Fig. 6.

Each packet is modeled as a bird with dynamic position and direction updates, which 'flies' over the network undergoing successive hop-by-hop transitions over discrete points in the 2D space, defined by the positions of hosting nodes. The set of sensor nodes comprises the environment where packets move. The sequence of transitions determines the packet's trajectory from its source to the sink.

Conceptually, in order to make moving packets behave like a flock, the basic characteristics of natural flocks discussed in the previous section are incorporated in the Flock-CC models. At each hop, a packet interacts with packets located on neighboring nodes in the FoV on the basis of attraction and repulsion forces, and experiences a 'gravitational' force in the direction of

[2]A recent study by Heyers et al. [19], strongly supports the hypothesis that migratory birds use their visual system to navigate using the magnetic field. In accordance with Heyers, the magnetic field or magnetic direction may be perceived as a dark or light spot which lies upon the normal visual field of the bird, and which, of course, changes when the bird turns its head.

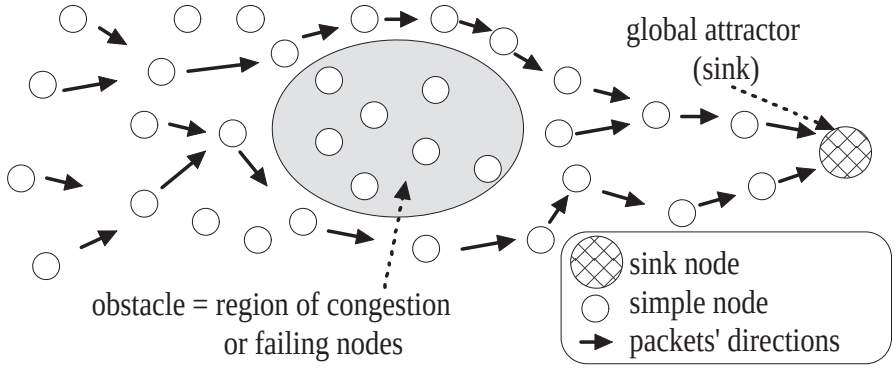

Fig. 6. Packet flock moving towards sink whilst avoiding 'obstacles'.

the sink (global attractor). More specifically, in the two Flock-CC models *packets are (a) repelled from neighboring packets located on nodes at close distance in the FoV (one hop away), (b) attracted to neighboring packets located on nodes at medium distance in the FoV (two hops away), (c) oriented and attracted to the global attractor under the influence of the environmental magnetic field*, and (d) experience some perturbation that may help the packets to pick a random route (i.e. trading exploration versus exploitation).

In this section, the basic elements of the both Flock-CC models are defined: (a) the repulsion and attraction zones and forces, (b) the artificial magnetic field, and (c) the field of view (FoV).

Before getting into details, consider a network of N autonomous nodes, $N > 0$, that are able to generate packets. Each node is associated with a finite queue, while node's throughput is constrained by the wireless channel capacity. A packet i and its hosting node $n \in \{1, .., N\}$ (i.e. packet i is residing in the queue of node n) are taken as points of reference in order to define and discuss repulsion and attraction zones, the notion of the field of view, and the direction of motion. The position of node n determines the position of the hosted packet i.

All quantities defined herein are regularly sampled at discrete time intervals of T seconds at each sensor node. Then, the values of these quantities are broadcasted periodically (every T seconds) to all neighboring nodes (within transmission range), using a dedicated control packet.

B. The first Flock-CC model: The basic elements

In the initial steps of developing the Flock-CC approach, a complex model [20], [1], [3], [2] was devised taking into account the repulsion and attraction forces, the artificial magnetic field, the FoV and randomness. The first model (Flock-CC v.1) involves 3 internal parameters (α, c, e). The complexity of the first model lies in selecting the optimal or compromise value for each parameter over a number of scenarios with different topologies and traffic conditions.

In this model, the zone of repulsion (ZoR) is related to the queue of each node l, and the zone of attraction (ZoA) to the wireless channel in the vicinity of each node l. This concept is illustrated in Fig. 7. The repulsion and attraction forces

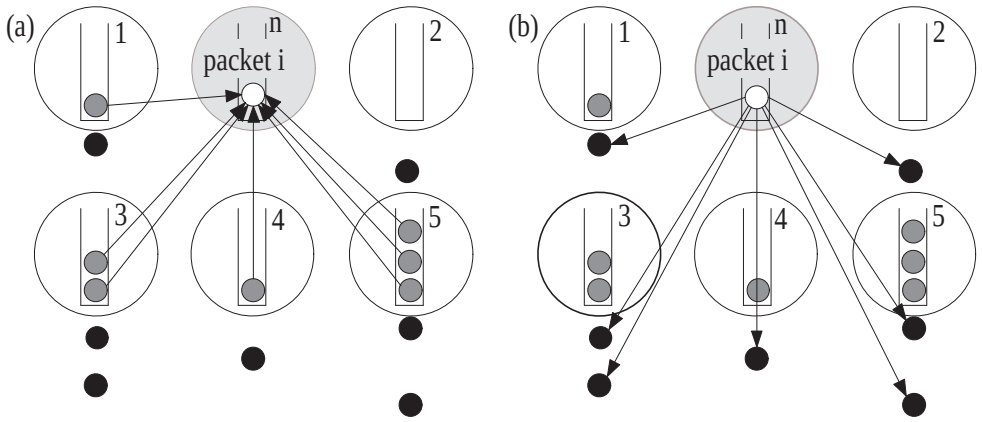

Fig. 7. The first Flock-based model: Forces exercised on packet i by neighboring packets located on each node l according to Flock-CC approach: (a) Repulsive forces, (b) Attractive forces. The dark grey shaded packets are in the ZoR (queues), while the black shaded packets are in the ZoA (wireless channel).

are defined on the basis of two new congestion indicators: the normalized queue node loading indicator and the normalized wireless channel loading respectively.

1) Repulsion force: The normalized node loading indicator combines the queue size, the incoming load and the outgoing load of a single node in order to capture the current congestion levels as well as to predict congestion. The normalized node loading indicator $p_l(k)$ at node l in the FoV is devised, given by the ratio:

$$p_l(k) = \begin{cases} 0, & \text{if } P_l^{in}(k) = 0, \\ & \text{and } P_l^{out}(k) = 0, \\ & \text{and } q_l(k^-) = 0; \\ \frac{P_l^{in}(k)+q_l(k^-)-P_l^{out}(k)}{P_l^{in}(k)+q_l(k^-)} & \text{otherwise.} \end{cases} \quad (1)$$

where $P_l^{in}(k)$ is the number of incoming packets, $P_l^{out}(k)$ is the number of successful outgoing packets, and $q_l(k^-)$ is the queue size at each node l. All parameters involved in this equation are measured at the end of every sampling period k, except for $q_l(k^-)$ which is obtained at the beginning of every sampling period k, in order to be able to determine the total number of packets traversing each node l within the sampling period.

The parameter $p_l(k)$, $0 \leq p_l(k) \leq 1$, reflects the ratio of the difference between the total number of packets to be served (packet arriving over period k, plus whatever was in the queue at the start of this period) minus the successfully transmitted packets, divided by the total number of packets to be served. From the perspective of the flocking behavior of birds, the parameter $p_l(k)$ represents the repulsion force exercised on packet i by packets traversing the queue (ZoR) of each node l at the kth sampling period. When $p_l(k) \to 0$, both the number of packet drops due to buffer overflows at node n is close to 0 and the queue is empty or nearly empty. On the other hand, as $p_l(k) \to 1$, node l is considered congested due to either a high number of packet drops, or high queue occupancy.

2) Attraction force: As a measure of the wireless channel loading, each node estimates the quality of the shared wireless channel using information taken from a CSMA-based MAC protocol. The total number of all packet transmission attempts at each node l (during sampling period k) is denoted by $P_l^{out*}(k)$, where $P_l^{out*}(k) = P_l^{out}(k)$+retransmits. The normalized wireless channel loading $r_l(k)$, at node l is denoted by:

$$r_l(k) = \begin{cases} 1 & \text{if retransmits}= 0 \text{ and } P_l^{out}(k) = 0; \\ \frac{P_l^{out}(k)}{P_l^{out*}(k)} & \text{otherwise.} \end{cases} \quad (2)$$

The parameter $r_l(k)$ ranges from 0 to 1 and represents the attraction force exercised on packet i by packets successfully transmitted through the wireless channel (ZoA), from each node l. When $r_l(k) \to 1$, the channel is not congested and a large percentage of packets are successfully transmitted (few packet retransmissions are observed). As $r_l(k) \to 0$, the channel is congested and a small number of packets are successfully transmitted, often after a large number of retransmissions.

Besides the repulsion and attraction forces, the fourth approach involves (a) the direction factor, $d_{il}(k)$ (Eq. 9), proposed for the equation-based artificial magnetic field of the second approach, as well as (b) the wide FoV shown in Fig. 11(b).

The desirability $D_l(k)$ for every node l in FoV is evaluated once in each sampling period k and is used for each packet sent within this period. It is given by

$$D_l(k) = g \cdot d_{il}(k) \cdot [\alpha \cdot r_l(k) + (1-\alpha) \cdot (1 - p_l(k))], \quad (3)$$

where the parameter g is a random variable that follows the Gaussian distribution with mean 1 and variance v, $g \sim N(1, v)$ and the parameter α, $0 \leq \alpha \leq 1$, regulates the influence of parameters $r_l(k)$ and $p_l(k)$. $D_l(k)$ measures the tendency of packets to move towards node l, which is proportional to low values of $p_l(k)$, and to high values of $r_l(k)$.

It can be deduced that nodes placed at equal hop distance from the sink can be selected if the noise perturbation g is sufficiently large to cover the bias against these nodes, that is introduced by the direction factor, $d_{il}(t)$. The probability with which this bias $1-e$ is covered depends on the standard deviation $\sqrt{v}$ of the Gaussian distribution. It makes sense to define v (and thus $\sqrt{v}$) not entirely independently of $1-e$, but as a linear function of $1-e$. Thus, let $v = c \cdot (1-e)^2$ (and thus $\sqrt{v}$ is linear in $1-e$). The value of c is varied in the experiments (and then v is computed), instead of varying v directly, since we believe that the parameters e and c are conceptually orthogonal and can be optimized independently. The experimental results support this choice.

After the evaluation of the desirability vector, the node m^* with the maximum desirability, is chosen as the new hosting node of packet i.

C. The second Flock-CC model: The basic elements

The second Flock-CC model (Flock-CC v.2) passed through three development stages. The various stages are presented below, starting from a simplistic model, Flock-CC v.2.1 (involving a small subset of the bird flocking characteristics), to more sophisticated (exhibiting better performance) models, Flock-CC v.2.2 and v.2.3, without deviating from the natural bird flocking behavior. The results presented in Section IV reveal the significance of each added element.

1) Repulsion and attraction zones and forces: The design of the second Flock-CC model was primarily motivated by the neighborhood-based model of Couzin et al. [4]. As discussed earlier, the second Flock-CC model is applied on a two dimensional topological (discrete) space defined by the graph of nodes. Each packet is allowed to move in a hop-by-hop manner, over a set of nodes along the path to the sink.

As shown in Fig. 8, the zone of repulsion is defined as a circle of radius R_t around packet i that includes all packets at close distance, i.e. within the transmission range of node n. Practically speaking, these packets reside in the queues of the grey-shaded nodes. On the other hand, the zone of attraction is the outer zone of 8 and includes all packets at medium distance from packet i. In practise, these packets reside in the queues of black-shaded nodes (two hops away from node n).

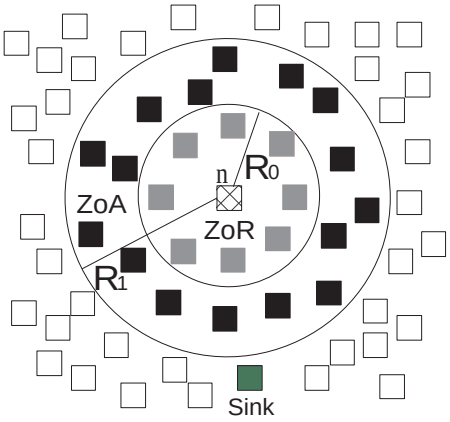

Fig. 8. Representation of a sensor network. R_0 is the transmission range of node n and defines an area (zone of repulsion) that includes all packets located on grey-shaded nodes. The outer area (zone of attraction) includes all packets located on black-shaded nodes.

The repulsive and attractive forces exhibited by packets on nodes one and two hops away respectively is proportional to the number of packets located on these nodes. The number of packets on nodes one hop away is directly obtained through control packets. Therefore, control packets are seen as means of transferring knowledge (propagate information) within the environment (sensor network) that is observable by birds' eyes.

On the other hand, in practise, the number of packets on nodes two hops away cannot be obtained timely through control packets since black-shaded nodes are outside the transmission range of the current hosting node. Thus, this number can be indirectly evaluated by measuring the number of packets[3] sent from nodes one hop away to nodes two hops away. Hence, packet i is repelled from packets residing in the queues of grey-shaded nodes and attracted to packets moving to black-shaded nodes. This idea is illustrated in Fig. 9.

2) Artificial magnetic field: In order avoid unnecessary routing loops and minimize packet loss, packets should be 'guided' to establish flight paths towards the sink. The role of the artificial magnetic field is twofold: provide orientation and attractiveness to the sink. Orientation to the sink is deduced from the direction of the magnetic field, while the attractiveness to the sink depends on the strength of the magnetic field (different on each direction, stronger in the direction of the sink). This behavior is apparent in migratory birds which fly polewards or equatorwards under the influence of the earth's magnetic field as shown in Fig. 10(a). In the Flock-CC model, the sink node can be seen as an artificial magnetic pole within the sensor network and packets are expected to 'fly sinkwards' under the influence of an artificial magnetic field as shown in Fig. 10(b).

The artificial magnetic field within the sensor network must point to the sink node. The direction of the sink can be determined on the basis of the hop distance parameter, $h_n(k)$, indicating the number of hops between each node n and the sink at the kth sampling period. Information about the hop distance to the sink is gradually propagated from the sink (pole) to each node into the network (environment where packets live) on the basis of control packets, having each node broadcasting its hop distance.

Each node perceives the direction of the magnetic field, and thus the sink node, through neighbors' proximity to the sink. Nodes located closer to the sink have smaller hop distances and are expected to be more attractive. Packets retrieve environmental information such as the artificial magnetic field from their hosting node. The arrows of Fig. 10(b) show the direction of the artificial magnetic field pointing to the sink node. The arrows mark the paths leading to the sink through nodes with descending hop distance.

The hop distance of a node may change due to network topology modifications caused by node failures or displacement. If node n does not hear control messages from a given neighboring node for a maximum of T_{lost} seconds, then the node n assumes that the neighbor has failed or gone out-of-range. In this case, the hop distance parameter of node n is re-evaluated if the loss of a neighboring node influences the parameter's value. Every change in hop distance values will be propagated

[3]These packets are easily perceived due to the broadcasting nature of the wireless channel.

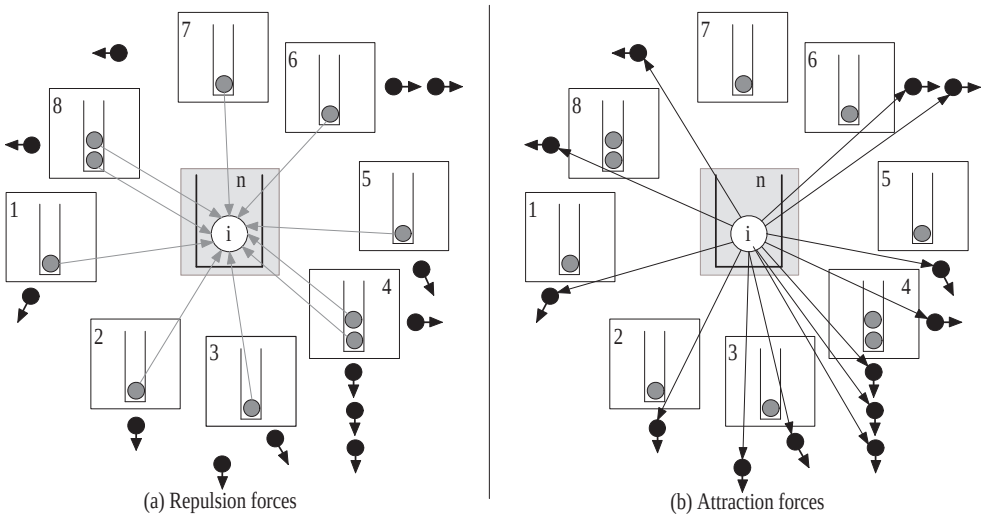

Fig. 9. Repulsion and attraction forces exhibited on packet i (on node n) from neighboring packets.

backwards within the network and all affected nodes are expected to update their hop related parameters. A detailed study of the hop distance protocol is beyond the scope of the current paper.

3) Field of view (FoV): Motivated by the limited visual perception of birds, packet i cannot 'see' and interact with all packets on nodes in its neighborhood (on nodes one and two hops away around its current hosting node) as in the simple model of Fig. 9. Packet i can perceive only a fraction of packets, these located in the FoV, i.e. in the observable world of the packet.

In general, the orientation of a bird's FoV can be set towards any direction, driving the movement of the bird accordingly. However, the orientation of a bird's FoV can be affected by the presence of magnetic fields. Migratory birds that need to travel polewards (or equatorwards) turn the orientation of their head, and thus their FoV, towards the pole (or the equator). In the same way, the FoV of packets can extend forward in the direction of the sink node as shown in Fig. 10(b).

The FoV may span from a few degrees up to 360^o. In the proposed approach, three different FoV apertures are considered as shown in Fig. 11. The *narrow FoV* includes only nodes with shorter hop distance to the sink, while the *wide FoV* consists of nodes with shorter or equal hop distance to the sink. In the extreme case, the 360-*degree FoV* of a packet includes all nodes in the neighborhood of the packet.

In this context, both the ZoR and the ZoA are redefined to involve the FoV. For example, in Fig. 10(b), packet i has a wide FoV. In this case, the ZoR is redefined as a circular zone of radius R_t, except for an area behind the packet i ('blind' area) that includes packets on nodes with longer hop distance than the current hosting node. The ZoR involves packets located on the heavy-gray shaded nodes of Fig. 10(b). Therefore, packet i is repelled from these packets as illustrated in Fig. 10(c). Similarly, the ZoA is the outer circular zone of Fig. 10(b) that includes packets on nodes at shorter or equal hop distance compared with the current hosting node (black-shaded nodes). Since the number of packets on black-shaded nodes is difficult

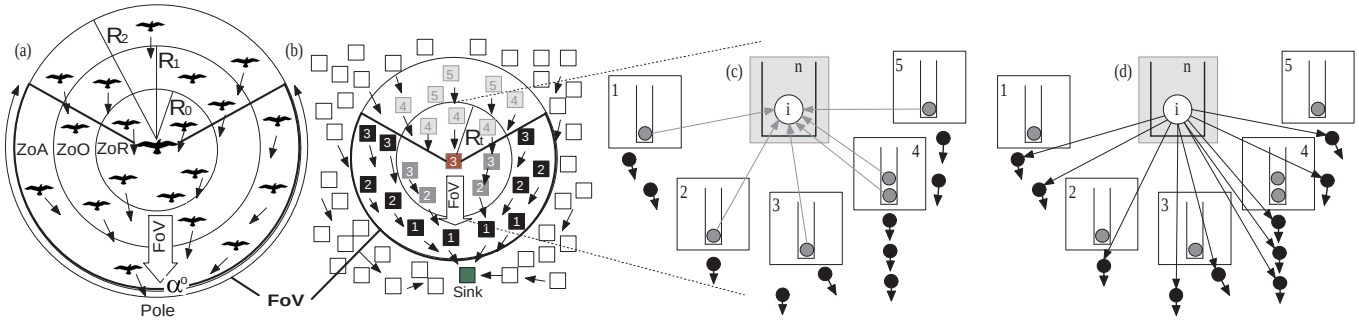

Fig. 10. (a) A bird flock moving polewards under the influence of the magnetic field of the Earth (black arrows). The FoV of the bird placed in the center extends forward in the direction of the magnetic pole. (b) Packets generated in a sensor network will move sinkwards under the influence of the artificial magnetic field (black arrows). The number on each node indicates the hop distance from the sink. The field of view (FoV) of packet i (on node n) extends forward in the direction of the sink. The ZoR and ZoA around packet i are redefined as circular zones, except for an area behind the packet i that is outside the FoV. (c) Repulsion forces exercised on packet i from packets in the ZoR (on heavy-gray-shaded nodes). (d) Attraction forces exercised on packet i from packets in the ZoA (moving to black-shaded nodes).

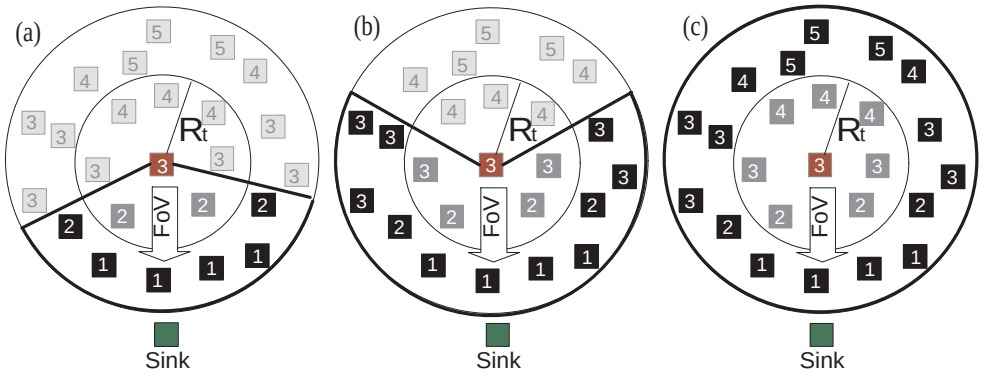

Fig. 11. (a) Narrow FoV including nodes with shorter hop distance to the sink. (b) Wide FoV including nodes with shorter or equal hop distance to the sink. (c) Complete 360-degree FoV.

to be timely obtained, packet i is attracted to packets moving towards these nodes.

4) Desirability function: The repulsive and attractive forces (exercised by packets one and two hops away respectively) are synthesized by the decision making process which is invoked by the hosting node of each packet. The synthesis of repulsive and attractive forces is captured through a desirability function. The decision making process results in selecting the most desired next hop node on the basis of avoiding or minimizing congestion phenomena on next hop nodes. The desirability function is evaluated once every sampling period and is used for each packet sent within this period.

D. Flock-CC v.2 development stages

This section presents the three development stages of increasing sophistication to mimic the flocking behavior of birds.

1) Flock-CC v.2.1: A simple idea is to have each packet i on node n of Fig. 8 repelled from packets on all grey-shaded nodes (one hop away) and attracted to packets on all black-shaded nodes (two hops away). The first development stage of the second model omits the notions of the field of view (actually this is identical to having a 360-degree FoV) the artificial magnetic field ('gravitational' force) towards the global attractor and randomness.

In each hop, packet i moves to a new hosting node from the set of grey-shaded nodes placed in the transmission range of its current hosting node n. Whenever packet i is about to be sent, the decision making process is invoked to determine the next hop node. Each hosting node evaluates the next hop node for each one of its packets based on an M-dimensional desirability vector, $\overrightarrow{D}(k)$, where $M \leq N$, is the number of nodes located within the hosting node's transmission range at the kth sampling period (it is evaluated once every sampling period). Each element, $D_m(k)$, of the vector $\overrightarrow{D}(k)$ represents the desirability for each node $m, m \in \{1, .., M\}$ in the transmission range of node n. The desirability $D_m(k)$ for every node m is evaluated once every sampling period k and is used for each packet sent from node n within this period. In the simplest form, $D_m(k)$ is given by:

$$D_m(k) = s_m(k) - q_m(k), \tag{4}$$

where $s_m(k)$ is the number of packets successfully transmitted from node m to nodes two hops away from node n (packets in ZoA) and $q_m(k)$ is the number of packets in the queue of node m (packets in ZoR). In the simplest case, the node m^* with the *maximum desirability* is chosen as the new hosting node of packet i.

Initial experimental results, on a network of 300 sensor nodes and a single sink node showed that less than 1% of packets were able to reach the sink. The problem is mainly attributed to two reasons.

The first reason is that packets are allowed to move in any direction *without orientation to a global attractor*. This causes high packet concentration in the network, especially in the vicinity of source nodes, because packets get trapped in loops. Eventually, the overwhelming majority of packets are lost due to collisions in the wireless channel. The second stage (Flock-CC v.2.2) incorporates the notion of orientation to the global attractor.

The second reason is that the decision making process does not employ perturbation when deciding a new hosting node. Thus, packets sent over the same sampling period move to the same new hosting node causing high queue occupancy on new hosting nodes. The third stage (Flock-CC v.2.3) investigates if and how perturbation influences the performance of the second Flock-CC model.

There was an attempt to face the problem of packets getting trapped in loops by introducing the notion of short-term memory in each packet. In this way, each packet was allowed to remember its last hosting node. The idea was to prevent packets from moving back to their previous location, so as to pick another route. Nevertheless, there was no remarkable improvement in experimental results.

2) Flock-CC v.2.2: Apparently, the simplistic model proposed in the first stage, Flock-CC v.2.1, simulated a 360-degree FoV, where packets were allowed to move in any direction. Unfortunately, the results were very negative but served as valuable feedback for further investigations. The second stage incorporates orientation to the global attractor by introducing the notions of the FoV and the artificial magnetic field.

The development of Flock-CC v.2.2 passed through several steps over which different options for (a) repulsion and attraction forces (with, or without normalization), (b) FoV aperture (narrow, or wide), and (c) magnetic field imposition (in determining FoV orientation, and in providing differentiated attractiveness to nodes in the FoV) were added to the model.

The model proposed in the second stage is progressively supplemented by a set of different features as follows:

1) Step 1: The influence of the artificial magnetic field is initially incorporated in the orientation of the FoV. Under the influence of the magnetic field, the FoV is seen to extend forward in the direction of the magnetic pole (sink) in order to guide packets 'fly' towards the sink.
2) Step 2: The attraction and repulsion forces involved in the desirability function are normalized to become comparable to each other.
3) Step 3: The attractiveness to nodes in the FoV is differentiated on the basis of the direction of the sink. In particular, stronger attractiveness to nodes closer to the sink is imposed. In this way, packets are expected to 'fly' over short paths to the sink, thus minimizing looping effects. The attractiveness to shortest paths is inherent in migratory birds which are seen to fly along the magnetic field lines. These lines travel the shortest distance from pole to pole.

In all scenarios, both the narrow and wide FoV (described in III-C3) are considered. In this way, the new desirability vector takes into account only packets located in the FoV of a packet that is ready to be sent. Again, the node with the maximum desirability is chosen as the new hosting node.

Step 1: The FoV extends forward in the direction of the magnetic pole as shown in Fig. 10(b). In the simplest case, moving packets are assumed to experience a homogeneous attraction to all nodes in the FoV overlooking the fact that the magnetic field (and thus attraction) is stronger in the direction of the pole (sink).

The expected number of nodes in the FoV (within both ZoR and ZoA) of packet i is denoted by L, $L \leq M \leq N$. Therefore, the desirability of each node $l, l \in \{1, .., L\}$ in the FoV, $D_l(k)$, is given by:

$$D_l(k) = s_l(k) - q_l(k). \tag{5}$$

Detailed experimental results on the 300-node topology are presented in the performance evaluation section, concerning 2 different FoV apertures: narrow and wide FoV. A first interpretation of the results for narrow and wide FoV showed a remarkable increase in the number of packets arriving at the sink compared to the scenarios of the first stage that do not consider the artificial magnetic field and the field of view.

Step 2: The values of parameters $s_l(k)$ and $q_l(k)$ may variate significantly for each node l. Therefore, normalization can be used to remove these undesirable variations and make parameter values more directly comparable. The *normalized desirability* of each node $l, l \in \{1, .., L\}$ in the FoV, $D_l^{norm}(k)$, is given by:

$$D_l^{norm}(k) = s_l^{norm}(k) - q_l^{norm}(k), \tag{6}$$

where

$$s_{nm}^{norm}(k) = \begin{cases} \frac{s_{nm}(k)}{s'_{nm}(k)} & \text{if } s'_{nm}(k) > 0; \\ \xi & \text{otherwise,} \end{cases} \tag{7}$$

and

$$q_l^{norm}(k) = \frac{q_l(k)}{Q}. \tag{8}$$

The parameter $s_l^{norm}(k)$ is the ratio of the successfully transmitted packets from node l, $s_l(k)$, divided by the total number of all packet transmission attempts[4] (including retransmissions) at each node l, $s'_l(k)$. The parameter $s_l^{norm}(k)$ can be seen as a measure of quality of the wireless channel loading around node l. The parameter $s_l^{norm}(k)$ ranges from 0 to 1 and represents the normalized attraction force exercised on packet i by packets moved (successfully transmitted) from each node l to nodes two hops away from node n (i.e packets within the ZoA). When $s_l(k) \to 1$, the channel around node l is not congested and a large percentage of packets are successfully transmitted (few packet retransmissions are observed). As $s_l(k) \to 0$, the channel is congested and a small number of packets are successfully transmitted, often after a large number of retransmissions.

An idle node l, i.e. with zero total transmission attempts, $s'_l(k) = 0$, does not provide any evidence of the wireless channel quality in its vicinity. Therefore, it cannot be said whether this node is either highly attractive, i.e. $s_l^{norm}(k) = 1$, or highly repulsive, i.e. $s_l^{norm}(k) = 0$. Parameter ξ_l is introduced as the normalized attraction force exercised by each node l that was previously idle ($s'_l(k) = 0$). High values of ξ are expected to result in *packet spreading* since packets will get attracted to idle

[4]We consider CSMA-like MAC protocols (e.g. IEEE 802.11) which employ a retransmission scheme to increase the reliability of the lossy wireless channel. A lost or erroneous packet is not retransmitted forever, but is dropped after a limited number of unsuccessful retransmission attempts.

nodes (most probably at the borders of the flock), whereas small ξ values may lead to *coherent flock motion*. The value of ξ_l in Eq. 7 is explored in performance evaluations.

The parameter $q_l^{norm}(k)$ reflects the ratio of the number of packets in the queue of node l divided by the queue capacity Q (assuming equal queue capacity for all nodes). The parameter $s_l^{norm}(k)$ is the percentage of queue occupancy at node l. The parameter $q_l(k)$, $0 \leq p_m(k) \leq 1$, represents the normalized repulsion force exercised on packet i by packets residing in the queue of each node l (i.e. packets within the ZoR). When $q_l(k) \rightarrow 0$, the queue is empty or nearly empty. On the other hand, as $q_l(k) \rightarrow 1$, node l is considered congested due to high queue occupancy. Based on the discussion above, the normalized desirability, $D_l^{norm}(k)$, ranges from -1 to 1.

Further experimental results on the same topology showed that normalization (step 3) gave significantly better results than new hosting node selection without normalization (step 2). Nevertheless, in scenarios with wide FoV, a large number of packets were trapped in loops between nodes of equal hop distance to the sink.

Step 3: A natural way to address the problem of packet loops is to insist on using the narrow FoV where packets are allowed to move only forward as shown Fig. 11(a). This natural solution is too rigid, as it artificially excludes consideration of other nodes which are not necessarily on the direct path, but may have higher desirability, and makes paths towards the sink 'too narrow', thus aiding contention and node loading as well as suppressing the ability of a packet to explore new paths. Furthermore, if the same nodes are always considered, then a higher power drain will be observed on these nodes and this may result in a shorter network lifetime. Furthermore, a problem may arise when front nodes either become unreachable (due to failures) or seen momentarily as unreachable (due to loss of control packets). In this case, packets reaching a dead end will be dropped.

The aforementioned considerations fueled the need for enhancing the second stage. In the third step of the second stage, besides keeping the wide FoV and the normalized desirability function for new hosting node selection, moving packets experience stronger attraction to nodes in the FoV located closer to the sink.

The wide FoV allows packets to be forwarded even to nodes that are placed at equal hop distance from the sink. However, some bias is applied against such a choice by discounting the desirability of equal hop distance nodes over the nodes that are closer to the sink (packet loops avoidance). Differentiated attractiveness to nodes in the FoV is done on the basis of the direction of the sink. The strongest attractiveness is experienced in the direction of the magnetic pole (sink), while attractiveness attenuates gradually as we deviating from the direction of the pole. Two different strategies were proposed for differentiating the attractiveness to nodes in the FoV: (a) equation-based, and (b) ruled-based evaluation.

In the *equation-based strategy*, the direction factor, $d_{il}(k)$, is introduced to regulate the attractiveness to nodes within the FoV:

$$d_{il}(k) = \begin{cases} 1 & \text{if } h_n(k) > h_l(k), \\ e & \text{if } h_n(k) = h_l(k). \end{cases} \tag{9}$$

where $h_n(k)$ is the hop distance of node n, and $h_l(k)$ is the hop distance of each node l at the kth sampling period. More specifically, $d_{il}(k)$ is set equal to 1 for all nodes l in the FoV that are closer to the sink than the hosting node n, and equal to some constant e, $0 \leq e \leq 1$, for all nodes l in the FoV at equal distance from the sink. The parameter e relates to the span of the FoV, that is, if $e = 0$ packets can move only to nodes closer to the sink. Therefore, the wide FoV degenerates into narrow FoV.

An *adjusted normalized desirability* of packet i for node l, $D'_l(k)$, can be evaluated by multiplying the direction factor, $d_{il}(k)$, with the normalized desirability $D_l^{norm}(k)$. However, this procedure is valid if $D_l^{norm}(k)$ is positive. For example, if $D_l^{norm}(k) < 0$ and $d_{il}(k) = e < 1$, then node l will become more desirable because its adjusted normalized desirability increases. Therefore, the adjusted normalized desirability of packet i for node l is defined as:

$$D'_l(k) = d_{il}(k) \cdot [D_l^{norm}(k) + 1] = d_{il}(k) \cdot [s_l^{norm}(k) - q_l^{norm}(k) + 1]. \tag{10}$$

Additional experimental results using the adjusted normalized desirability showed an even greater increase of the number of successfully delivered packets, thus confirming the importance of using the direction factor. A high increase in packet delivery ratio was observed for $e = 0.25 - 0.5$ and $\xi = 0.75 - 1$. On the other hand, a slight decrease in PDR was shown for $e = 0$ due to problems related to the narrow FoV, and are explained in detail in the evaluations section.

A simplified, *rule-based strategy* for differentiated attractiveness can be followed when choosing the new hosting node. The rule-based strategy is simpler than the equation-based strategy since only one parameter (ξ) is used. After the evaluation of the normalized desirability, $D_l^{norm}(k)$, for each node l in the FoV:

1) Choose the node with the maximum desirability and available buffer space from nodes *closer* to the sink as the new hosting node $\rightarrow$ packet goes forward.
2) When all nodes closer to the sink either have no available buffer space or are seen to be unreachable, choose the node with the maximum desirability and available buffer space from nodes at *equal hop distance* to the sink as the new hosting node $\rightarrow$ packet goes side-ways.
3) Otherwise, choose the node with the maximum desirability and available buffer space from nodes at *longer hop distance* to the sink as the new hosting node $\rightarrow$ packet goes backwards.

TABLE I
THE FIRST FLOCK-CC MODEL AND THE THREE DEVELOPMENT STAGES OF THE SECOND FLOCK-CC MODEL.

Model	*Repulsion and Attraction*	*Field of view*	*Magnetic field*	*Randomness*
Flock-CC v.1	yes (with normalization)	wide	yes (equation-based)	yes (gaussian distribution)
Flock-CC v.2.1	yes (without normalization)	360^o	no	no
Flock-CC v.2.2	yes (with/without normalization)	narrow/wide	no/yes (equation-based/rule-based)	no
Flock-CC v.2.3	yes (with normalization)	wide	yes (rule-based)	yes (roulette wheel/rank-based)

The rule-based approach exhibited significantly better results compared to the equation-based approach. More detailed results are given in the performance evaluation section.

3) Flock-CC v.2.3: As initially discussed, randomness is that part of nature which allows for exploration, and perhaps identification of better solutions. Randomness is included in the rule-based strategy by introducing some noise when choosing a new hosting node. This process is expected to tackle the problem of packet transitions to the same (highly desirable) new hosting nodes within the same sampling period which emerges when focusing on maximum desirability.

Perturbation can be employed by randomly selecting a new hosting node. However, in order to provide a fair way of selection, the probability of selecting a node should be proportional to the desirability of that node. This process is captured by selection methods used in genetic algorithms as for example, roulette wheel selection, rank selection and tournament selection. Selection methods are used for randomly selecting members from the population of chromosomes with probability proportional to their fitness. *In the proposed approach, desirability is seen as the fitness of each potential new hosting node*.

In roulette wheel selection, if f_i is the fitness of individual i in the population, then its probability of being selected is:

$$p_i = \frac{f_i}{\sum_{j=1}^{J} f_j}, \tag{11}$$

where J is the number of individuals in the population. The proposed approach uses the population of all nodes in the FoV, i.e. $J = L$. Roulette wheel selection cannot be directly used with negative fitness. Recall that $D_l^{norm}(k)$ ranges from -1 to 1. Thus, the normalized desirability is shifted by adding 1 to range from $0-2$ to as to be used in Eq. 11. The main disadvantage of this method is when the fitnesses differ very much. For example, if the best individual fitness is 90% of the entire roulette wheel then the other individuals will have very few chances to be selected.

These problems can be mitigated by using rank selection to modify the value of each fitness. Rank selection ranks each individual and a fitness value is assigned according to the rank it receives. The weakest individual receives the value of 1, the second worst receives the value of 2, etc. and the fittest individual receives the value of J. The probability of an individual to be selected is equal to the fitness of the individual divided by the total fitness of all the individuals, as in Eq. 11.

These selection methods were used in performance evaluations and the results are presented in the next section.

E. Design parameters

The parameters T, ξ, α, e and c are control parameters of the two Flock-based congestion control models discussed in this section. The parameter T is involved in both models and represents the sampling period for parameters $s(k)$, $q(k)$, $p(k)$ and $r(k)$ and the control packet broadcasting period. T is expected to have a significant impact on the performance of all approaches. The parameter α is involved in the first model and regulates the influential roles of the node loading indicator $p_m(k)$, and the wireless channel loading indicator $r_m(k)$ on the desirability function of Eq. 3. The parameter ξ is involved in the second model and measures the attractiveness of previously inactive nodes in the evaluation of the normalized desirability. The parameter e is involved in the second model and is used to regulate the attractiveness to nodes within the FoV placed at equal hop distance form the sink. The parameter c trades off exploration versus exploitation in the first model. All these parameters need to be carefully selected. Their selection is further discussed in the evaluation section.

IV. PERFORMANCE EVALUATION

This section evaluates the performance of the two Flock-CC models through simulation studies conducted using the ns-2 network simulator [21], and discusses the effectiveness of each model in combating congestion by mimicking the collective behavior of bird flocks.

Performance evaluations focused on 3 directions. The first direction was to experiment with the two proposed Flock-based congestion control models on the basis of *parameter selection* and comparative evaluation among them, which drive the selection of the most efficient and effective approach. Table I summarizes the four proposed approaches from a comparative perspective.

The second direction refers to the *demonstration of emerging behavior*, *self-adaptation*, and *robustness against failing nodes* of the two Flock-CC models. Finally, the both Flock-based models were compared with related (nature-inspired and conventional) congestion control approaches.

A. Evaluation parameters

The two models were evaluated using similar topologies and scenarios of operation as well as the same measures of performance. All these issues are discussed below.

1) Topologies: The 2D lattice topology was used in the overwhelming majority of scenarios for both models so as to better understand and evaluate the behavior of the proposed models. In this kind of topology, neighboring nodes were placed at the same distance ($25 \cdot \sqrt{2}$m) from each other, in such a way that each node has at most 8 neighboring nodes one hop away. In order to experiment with more realistic topologies, both models were evaluated in a random topology as well.

All nodes were homogeneous and identical in hardware and software setup. The radio propagation range of each node was 50m. A two-ray reflection propagation model was used which accounts for the effect of multipathing and fading. The radio model assumes that the radio can lock onto a sufficiently strong signal in the presence of interfering signals. The control packet size and the data packet size were set to 10 and 50 bytes respectively. The CSMA-based IEEE 802.11 MAC protocol, provided in the ns-2 simulator, with an exponential backoff policy was adopted, having RTS/CTS packet exchanges disabled for energy saving and low signalling overhead purposes. Two transmission rates of 2 Mbps and 250 Kbps were used. In the former case, the queue size of each node was set to 50 packets, while in the latter case was set to 15 packets.

Flock-CC v.1: The two lattice topologies used for evaluating Flock-CC v.1 consisting of 200 and 400 homogeneous sensor nodes are shown in Fig. 12. The random topology for the Flock-CC v.1 consists of 400 homogeneous nodes deployed in a uniform random manner.

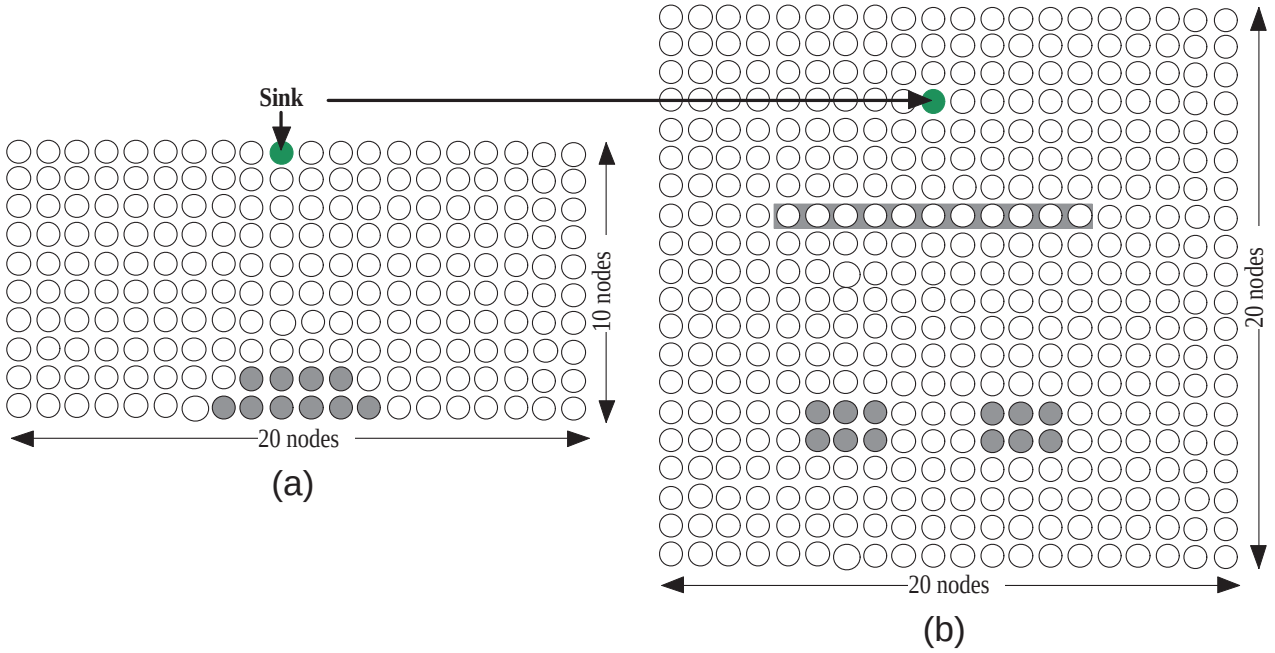

Fig. 12. Evaluation topologies: (a) 200 nodes, (b) 400 nodes.

Flock-CC v.2: The two lattice topologies for Flock-CC v.2 consist of 300 nodes as shown in Figs. 13(a) and (b). In the random topology for the Flock-CC v.2, the set of 300 nodes was deployed in a uniform random manner.

2) Scenarios: **Flock-CC v.1**: A number of representative network operation scenarios were defined for evaluating Flock-CC v.1. In each scenario, different sets of nodes were activated.

In the *first scenario* (scenario 1), (used for parameter evaluation) the heavy grey shaded nodes of Fig. 12(a) located in the middle bottom part of the network were activated.

The *second and third scenarios* (scenarios 2 and 3) demonstrate the self-adaptiveness and the robustness of the proposed mechanism against failing nodes. In the second scenario, the heavy grey shaded nodes located in the bottom part of the network of Fig. 12(b) were activated. In the third scenario, the same nodes as in the second scenario were initially activated, while 11 nodes located within the heavy grey shaded zone (in the middle of the network) failed at $t = 60$ secs. The duration of all scenarios was 100 secs.

The *fourth scenario* (scenario 4) involved the activation of 10 nodes placed in the same neighborhood, 7 hops away from the sink. In practise, it is quite common to have nodes closely located to each other being activated almost at the same time when an external stimulus (event) is detected.

Flock-CC v.2: In order to investigate all the different aspects (parameter selection, self-adaptation, emerging behavior, robustness) of the second model, a series of representative network operation scenarios were defined. Each scenario corresponds

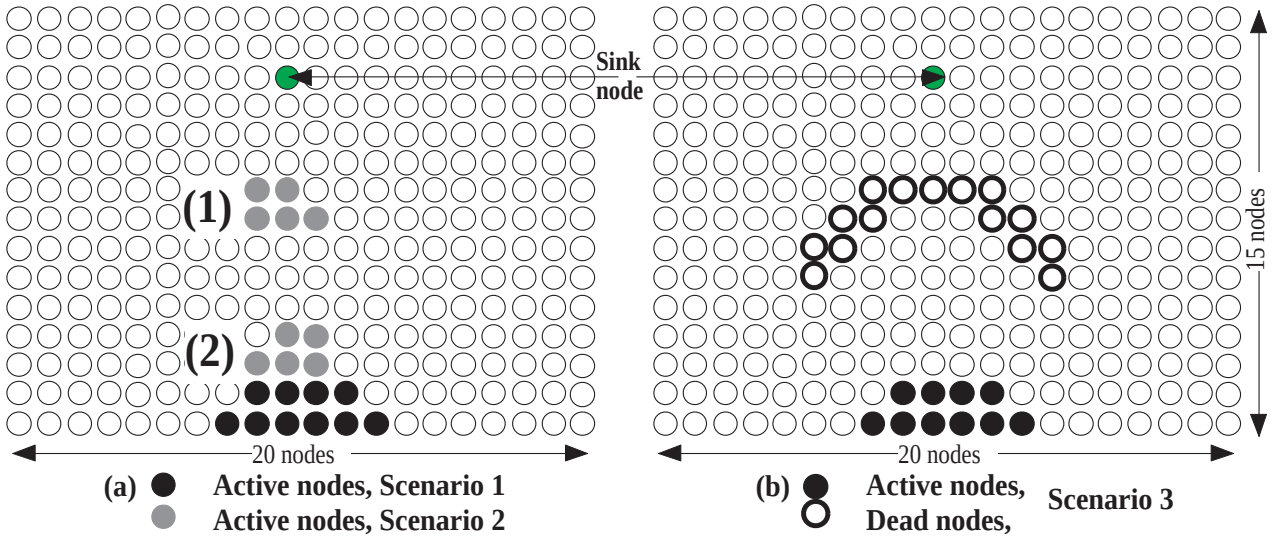

Fig. 13. Evaluation topology and scenarios.

to events occurring in different locations, having different sets of nodes being activated for sending packets. The first three scenarios are related to the 2D lattice topology, while the fourth scenario concerns random topologies. In all scenarios, sets of closely located nodes were sending packets. In practise, it is quite common to have sending nodes closely located to each other being activated almost at the same time when an external stimulus (event) is detected.

In the *first scenario* (scenario 1), 10 black shaded nodes located in the middle bottom part of Fig. 13(a) were sending packets. This scenario was used for parameter setting evaluations and comparisons among the proposed approaches.

The emerging behavior and the self-adaptiveness of all proposed approaches were evaluated on the basis of the *second scenario* (scenario 2). In this scenario, the front set of 5 grey shaded nodes of Fig. 13(a) (close to the sink) were initially sending packets. In this way, a congestion region (of heavily loaded queues and wireless channel) was created around and in front of the sending nodes towards the sink. In order to demonstrate the ability of the flock-based approach to manoeuvre around the congestion region, the back set of 5 grey shaded nodes started sending packets at $t = 50$s. Eventually, the front set of nodes stopped sending packets at $t = 70$s.

The *third scenario* (scenario 3) was used to demonstrate the robustness of the proposed approaches against failing nodes, even under extremely undesirable situations. In this scenario, the black shaded nodes located in the bottom part of the network of Fig. 13 (b) were initially sending packets (as in the first scenario), while bold circled nodes in the middle of the network failed at $t = 40$s.

Finally, the *fourth scenario* (scenario 4) was used to demonstrate the ability of the proposed approaches to perform well when the underlying sensor network infrastructure is random. The evaluation scenario involved the activation of 10 sender nodes placed in the same neighborhood, around 7 hops away from the sink.

3) Variables: The design parameters ξ, α, e and c were chosen to range from 0 to 1. The time between successive control packets, T (sampling period), was assigned the values $0.5, 1.0, 1.5$ and 2.0s in all approaches. The selection of T to be less than or equal to 2s is guided by the desire to maintain responsiveness to changes in the network state. It is also desirable to avoid overwhelming the network with control packets, thus T should not be very low. The parameter T_{lost} concerning the loss of communication with a certain neighbor was set to $3T$.

Each sender node was allowed to generate constant bit rate (CBR) traffic at the rates of either 25 (low load), or 35 (medium load), or 45 (high load) pkts/s (all nodes at the same rate, different for each scenario) when triggered by an event. These three cases can be considered as slightly congested, congested, and heavily congested, respectively.

4) Measures of performance: Three performance measures for congestion control approaches were taken into account: the packet delivery ratio (PDR), the end-to-end delay (EED), and the energy tax. Packet delivery ratio is defined as the ratio of the total number of packets received by the sink to the total number of packets transmitted by source nodes. End to end delay is defined as the time taken for a packet to be transferred from a source node to the sink. The energy tax metric calculates the average energy consumption per node per delivered packet, measured in mJoules/delivered packet at the sink.

B. Parameter selection

This section evaluates the performance of the two proposed flock-based congestion control models, providing parameter selection and performing comparative evaluation among them.

Each scenario, concerning different combinations of parameter values, was executed 10 times and the mean values of the metrics over all scenarios are presented below. In some figures, the mean values are supplemented with 95% confidence intervals were needed.

1) Flock-CC v.1: Fig. 14 illustrates the impact of α, e and c on PDR for the transmission rates of 35pkts/sec (i.e. the network can be considered congested) for scenario 1. Parameter T was set to 1 sec. As can be seen, the combinations of values $0.4 \leq \alpha \leq 0.8$, $0.5 \leq e \leq 0.7$ and $0.5 \leq c \leq 0.75$ resulted in high PDR (around 85%). The highest PDR (dashed line) was achieved for $\alpha = 0.4, e = 0.6$ and $c = 0.5$.

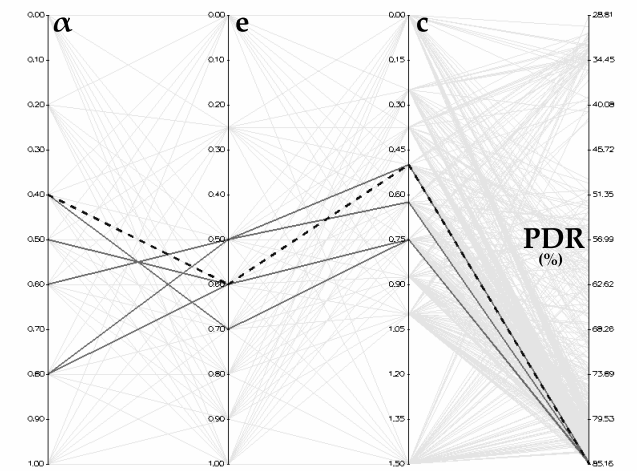

Fig. 14. Flock-CC v.1: Packet delivery ratio (PDR) in scenario 1 when the transmission rate is 35 pkts/sec.

For low values of α (i.e. less than 0.4), the useful link service rate, r_n, was not taken into consideration. Thus, PDR was decreased as a result of collision effects that were omitted. On the other hand, the increase of α amplified the tendency (attraction) of packets to move towards nodes experiencing low channel utilization within the perception field (i.e. to move at the borders of the flock) in order to avoid collision hot spots occurring inside the network. For high values of α beyond 0.8, the influential role of parameter r_n in the desirability function was enhanced. Thus, packets were caught in loops between nodes experiencing low channel utilization, resulting in low PDR values. Based on the results of Fig. 14, the parameter α could be set between 0.4 and 0.8.

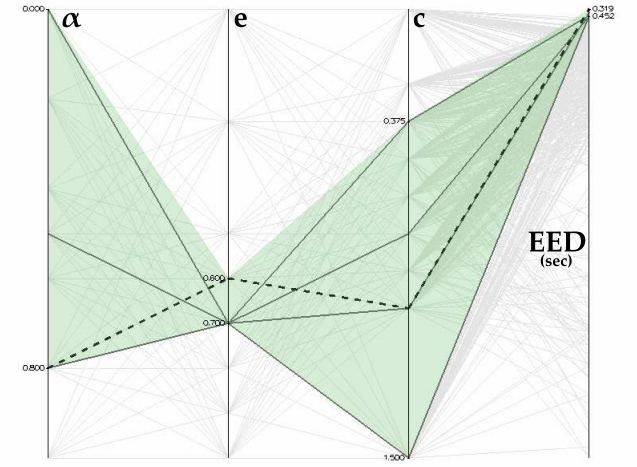

Fig. 15. Flock-CC v.1: End-to-end delay (EED) in scenario 1 when the transmission rate is 35 pkts/sec.

As stated before, parameter e determines the bias against nodes at equal hop-count from the sink. When e was between 0 and 0.4, the field of perception of each packet was narrow because packets preferred moving towards nodes located closer to sink. On the other hand, for $e > 0.7$, nodes were allowed to move towards nodes with equal hop-count with high probability. As shown in Fig. 14, PDR deteriorated for $e > 0.7$ because packets were caught in loops between uncongested nodes, causing excessive packet loss attributed to wireless channel collisions. Based on Fig. 14, the parameter e could be set between 0.5 and 0.7.

As far as parameter c is concerned, Fig. 14 shows that higher PDR values were obtained when $c \neq 0$, due to the randomized selection of nodes within the perception field, resulting in traffic spreading. Based on these results, parameter c could range from 0.5 to 0.75.

Fig. 15 illustrates the impact of α, e and c on the end-to-end delay (EED) for scenario 1. As can be observed, the fastest transitions of packets to the sink were exhibited for $\alpha = 0.8, e = 0.6$ and $c = 1$. However, low EED values were also achieved for parameters' values within the shaded area of Fig. 15 (including the optimal values for PDR).

Fig. 16(a) highlights that $a = 0.4, e = 0.6$ and $c = 0.5$ offer consistently the best behavior for scenario 1, while similar results were obtained for $a = 0.5, e = 0.6$ and $c = 0.75$. Based on all the experimental results presented thus far, the optimal combination of the design parameters values achieving high PDR and low EED, regarding the scenario under study, was $a = 0.4, e = 0.6$ and $c = 0.5$.

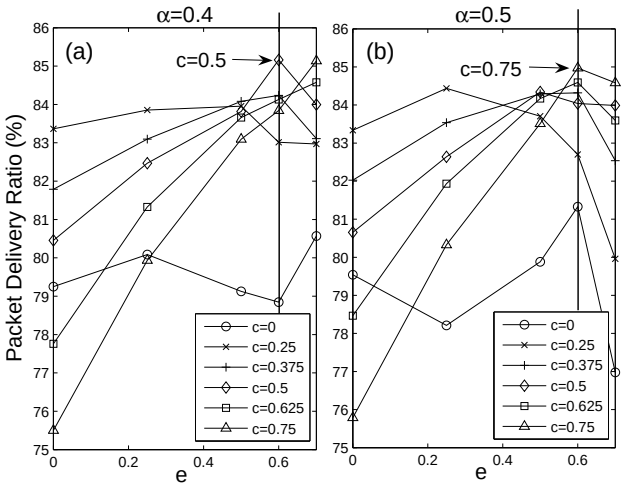

Fig. 16. Flock-CC v.1: Packet Delivery Ratio (PDR) in scenario 1 when the transmission rate is 35 pkts/sec (detailed results for $\alpha = 0.4, 0.5$) .

Fig. 17 illustrates the impact of α, e and c on energy tax at 35pkts/sec for scenario 1. As can be seen, the lowest energy tax (0.026mJ/delivered packet) was obtained for $\alpha = 0.5, e = 0.6$ and $c = 0$ (dashed line of Fig. 17).

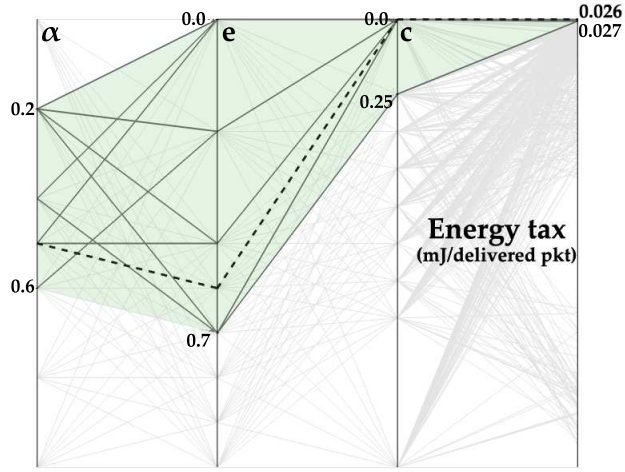

Fig. 17. Flock-CC v.1: Energy tax (in mJ per delivered packet) in scenario 1 when the transmission rate is 35 pkts/sec.

Similarly, low energy tax levels were achieved for $0.2 \leq \alpha \leq 0.6$, $0 \leq e \leq 0.7$ and $0 \leq c \leq 0.25$. As stated before, parameter e determines the bias against nodes at equal hop-count from the sink. When $e = 0$ packets can only move towards nodes located closer to sink (high flock coherence). On the other hand, as e approaches to 1, packets are allowed to move towards nodes with equal hop-count with high probability (high traffic spreading). Perturbation is regulated by the parameter c. When e and c were close to 0 (i.e. high packet flock coherence and low perturbation), packets were moving on narrow paths to the sink resulting in low energy consumption per node. On the other hand, high packet spreading was observed for $e \rightarrow 1$ or $c \rightarrow 1$ causing transition loops of packets between uncongested nodes and, as a result, high energy consumption. Also, Fig. 17 shows that high energy consumption was observed for $\alpha > 0.6$. The increase of α, amplified the tendency of packets to

move towards nodes experiencing low channel utilization (i.e. at the borders of the flock) in order to avoid collision hot spots occurring inside the network. However, packets were caught in loops between nodes experiencing low channel utilization, resulting in high energy consumption.

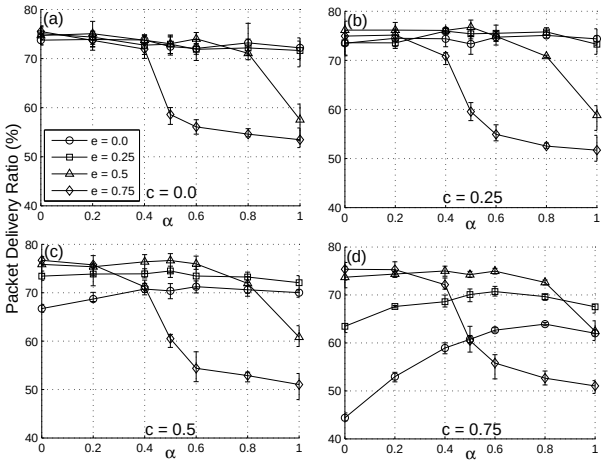

Fig. 18. Flock-CC v.1: Packet Delivery Ratio (PDR) in scenario 4 (random topology) when the transmission rate is 35 pkts/sec.

Fig. 18 illustrates the impact of α, e and c on packet delivery ratio (PDR) for scenario 4. As shown in Fig. 18, PDR deteriorated for $e \geq 0.75$, because packets were caught in loops between neighboring nodes, causing excessive packet loss attributed to both wireless channel collisions and buffer overflows (see Fig. 19). As can be seen, a higher PDR was achieved when $alpha = 0.5$, $e = 0.5$ and $c = 0.25$ or $c = 0.5$. When $c = 0$, the non-randomizing selection of new hosting nodes did not allow packets to exploit all the available paths to the sink causing a high number of buffer overflows (see Fig. 19). On the other hand, large values of c (high randomization) resulted in low PDR values, because packets were trapped in loops.

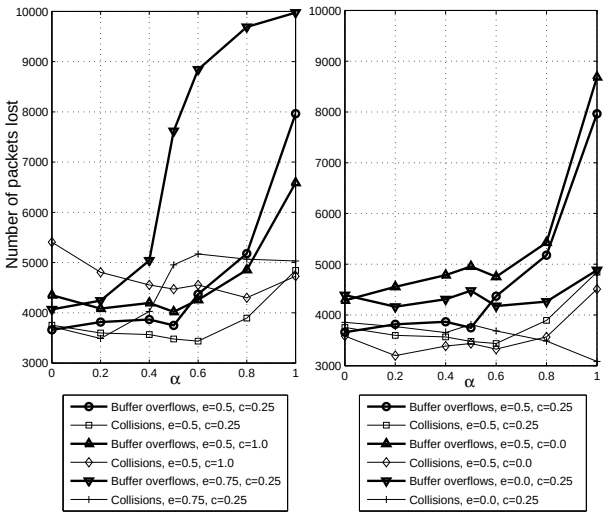

Fig. 19. Flock-CC v.1: Number of packet lost due to collisions and buffer overflows in scenario 4 (random topology) when the transmission rate is 35 pkts/sec.

The good compromise choice of $\alpha = 0.5$ allows for a balanced influence of parameters r_m and p_m on the desirability function of Eq. 3. When $\alpha < 0.5$, the selection of a new hosting node is governed by the queue node loading indicator p_m without taking into account the wireless channel conditions in the vicinity of each potential hosting node. On the other hand, an increase of α beyond 0.5 minimizes the influence of p_m on the desirability function. Thus, the repulsion forces from nodes with high loading decay, and packets are not prevented from moving towards 'crowded' nodes (causing high buffer overflows). Further evaluation results showed that the same behavior was exhibited for both lower and higher traffic load at the rates of 25 and 45 pkts/s respectively.

Fig. 19 displays the number of packets lost due to collisions and buffer overflows when active nodes send at 35 pkts/s for different combinations of parameters α, e and c in scenario 4. It can be observed that for the majority of combinations of e and

c values, the number of buffer overflows was greater than the number of collisions. In networks with random node deployment, there might not exist a large number of available paths to the sink, thus packets are traversing the network through a small number of alternative paths. Therefore, the buffers of nodes involved in these paths are frequently overwhelmed by packets leading to buffer overflows. It can be observed that the smallest number of packets lost (cumulatively due to collisions and buffer overflows) was achieved for $\alpha = 0.5, e = 0.5$ and $c = 0.25$. This combination of e and c parameters was compared against extreme values of e and c, keeping one of these parameters to its best case value. Remarkably high packet losses occurred for $e = 0.75$ (collisions + buffer overflows) due to the looping behavior of packets inside the network as shown in Fig. 19(a). On the other hand, low packet losses were observed for $e = 0$ in Fig. 19(b) because the narrow field of view disabled high packet spreading, and thus packet looping. Also, a high number of buffer overflows was observed with an increase of α (beyond a certain value, different for each scenario, but mostly greater than 0.5) for the reason described above.

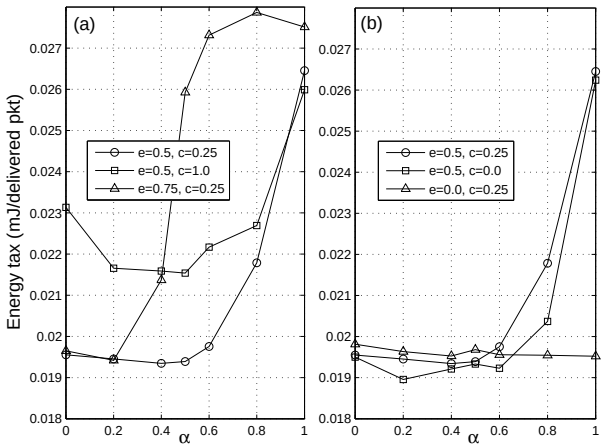

Fig. 20. Flock-CC v.1: Energy tax (in mJ) per delivered packet in scenario 4 (random topology) when the transmission rate is 35 pkts/sec.

Fig. 20 presents the energy tax paid in mJ per delivered packet for certain combinations of parameters α, e and c in scenario 4. It can be observed that the lowest energy tax was paid for the combination $\alpha = 0.2, e = 0.5$ and $c = 0$ but this was at the expense of lower PDR. As shown in Fig. 19(b), the low energy tax was attributed to the low number of collisions, and thus to the low number of retransmissions at the MAC layer. Also, low energy tax was paid for the combination $\alpha = 0.5, e = 0.5$ and $c = 0.25$ which achieved good compromise in terms of PDR and EED. It is also apparent that a large amount of energy was consumed when $e = 0.75, c = 0.25, \alpha > 0.2$ and $e = 0.5, \alpha > 0.6$ due to the vast number of retransmissions of packets that were lost due to buffer overflows (mostly) and collisions.

Based on the experimental results for scenario 4 (random topology), a good compromise combination of the design parameters values achieving a good behavior in terms of high PDR and low EED was $a = 0.5, e = 0.5$ and $c = 0.25$.

2) Flock-CC v.2.1: The performance of the first approach, which does not involve any parameters, was evaluated on the basis of the first scenario for $T = 0.5, 1, 1.5, 2.0$s and traffic rates of $25, 35$ and 45 pkts/s. All the results showed that less than 1% of packets were able to reach the sink. The problem is mainly attributed to two reasons. The first reason is that packets are allowed to move in any direction without any orientation to a global attractor. This causes high packet concentration in the network, especially in the vicinity of source nodes, because packets get trapped in loops. Eventually, the overwhelming majority of packets are lost due to collisions in the wireless channel. The second problem is that the decision making process does not employ perturbation when deciding a new hosting node. Thus, packets sent over the same sampling period move to the same new hosting node causing high queue occupancy on new hosting nodes.

There was an attempt to face the problem of packets getting trapped in loops by introducing the notion of short-term memory in each packet. In this way, each packet was allowed to remember its last hosting node. The idea was to prevent packets from moving back to their previous location, so as to pick another route. Nevertheless, there was no remarkable improvement in experimental results.

3) Flock-CC v.2.2: The results of the second stage of the second model are divided into three categories depending on the different features added to the model on each step of Section III-D2. The first two steps were evaluated on the basis of the first scenario, while in the third scenario (rule-based) all three scenarios of Fig. 13 were used. All simulations were performed for $T = 0.5, 1, 1.5, 2.0$s and traffic rates of $25, 35$ and 45 pkts/s.

Step 1: Fig. 21 depicts the PDR for both narrow and wide FoV, for different traffic rates ($25, 35$ and 45 pkts/sec) and as T changes from 0.5 to 2s. A first observation of the results reveals a remarkable increase in PDR (from 15% to 70%) in all scenarios compared to the first stage. This outcome underlines the importance of the magnetic field which imposes orientation to the sink as well as the need for limited FoV that prevents packets from deviating from the paths leading to the sink.

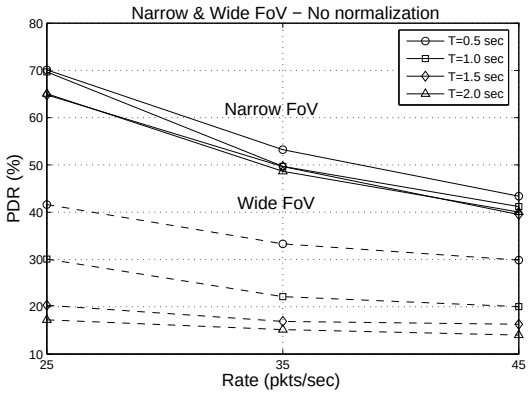

Fig. 21. Flock-CC v.2.2, step 1 (orientation of FoV): Packet Delivery Ratio (PDR) for narrow and wide FoV.

A closer view of Fig. 21 shows that scenarios with narrow FoV achieved higher PDR compared to scenarios with wide FoV. In scenarios with narrow FoV, packets were 'guided' to traverse nodes with shorter hop distance to the sink. Due to the narrowness of the perception field, the flock of packets was moving on a coherent formation (figure) over the shortest paths to the sink. The coherent movement of packets over the shortest paths resulted in the decrease of packet loss. However, the drawback of this approach was that alternative paths through nodes along longer paths to the sink were left unexploited. On the other hand, scenarios involving wide FoV achieved lower PDR as a result of high traffic spreading among multiple paths to the sink. The poor performance was also attributed to the homogeneous attractiveness to nodes in the FoV. The homogeneity of attractiveness did not impose any preference to nodes along the shortest paths to the sink in order to 'force' packet flocks flow towards the destination. Thus, a large number of packets trapped in loops. The considerations of this paragraph are reflected in Fig. 22.

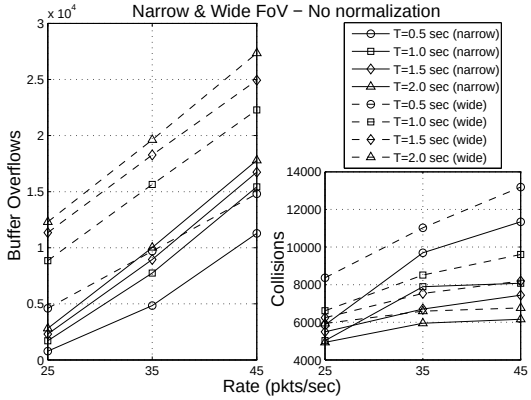

Fig. 22. Flock-CC v.2.2, step 1 (orientation of FoV): Packet loss for narrow and wide FoV.

Fig. 22 displays the number of packets lost due to channel collisions and buffer overflows for different combinations of traffic rates and T and for both narrow and wide FoV. The majority of packet loss was attributed to buffer overflows (up to 3 times more than collisions). It is apparent that narrow FoV displayed lower packet loss than wide FoV due to both buffer overflows and collisions for all traffic rates and T values as explained in the previous paragraph. In addition, the number of buffer overflows rose with the increase of T, whereas the number of collisions rose with the decrease of T. Recall that the desirability function was evaluated once every sampling period, and packets to be sent within this period chose the most desirable node. At high T values, where the desirability function was evaluated more infrequently, packets tended to choose the same new hosting node over a longer time period (no randomness was applied) leading to overloading (high queue occupancy) of the chosen node. On the other hand, at low T values, packets spread more frequently to different new hosting nodes eliminating buffer overloading but causing increase of channel collisions around the chosen nodes.

As shown in Fig. 22, the lowest *cumulative* packet loss (due to collisions and buffer overflows) for every traffic rate was achieved for $T = 0.5$s. Therefore, it can be deduced that at low T values the proposed approach maintains responsiveness to changes in traffic load, but at the cost of added control packets.

Fig. 23 illustrates the impact of parameter T on EED for both narrow and wide FoV, for the different traffic rates. It is worth pointing out that only packets delivered at the sink were taken into account in EED evaluations. As can be observed,

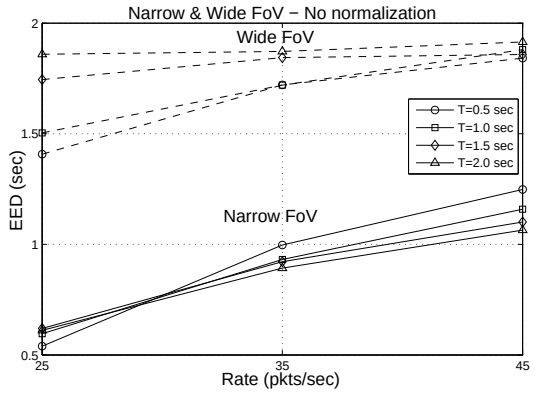

Fig. 23. Flock-CC v.2.2, step 1 (orientation of FoV): End to end delay (EED) for narrow and wide FoV.

the fastest transitions of packets to the sink were exhibited for scenarios with narrow FoV since packets traversed the shortest paths to the sink. In narrow FoV scenarios with medium and high traffic loads, the highest delay was observed for $T = 0.5$s. since network resources (buffer and channel capacity) were highly overloaded. In wide FoV scenarios, conclusions cannot be safely extracted since the majority of packets were lost.

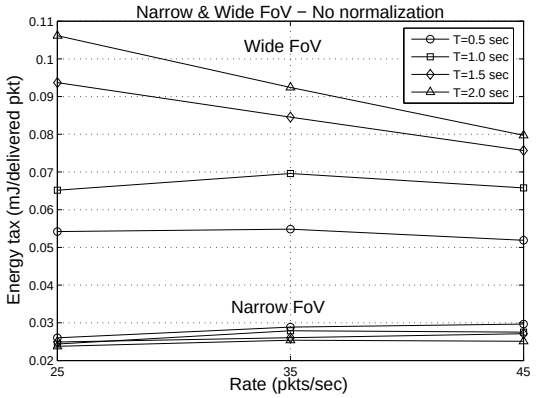

Fig. 24. Flock-CC v.2.2, step 1 (orientation of FoV): Energy tax for narrow and wide FoV.

Fig. 24 presents the energy tax paid per delivered packet for both narrow and wide FoV, for the different traffic rates. The results are quite similar to those obtained for EED (Fig. 23). More specifically, low energy tax (< 0.03mJ/delivered packet) was paid for narrow FoV scenarios. In contrast, larger amount of energy ($0.05 - 0.11$mJ/delivered packet) was consumed in wide FoV scenarios due to the vast number of retransmissions of packets attributed to high packet loss (collisions + buffer overflows).

Step 2**:** Further improvement of Flock-CC v.2.2 was carried out by normalizing the attraction and repulsion forces involved in the desirability function, as expressed by Eq. 6. The parameter ξ involved in the evaluation of the normalized attraction force, $s^{norm}(k)$, was selected to range from 0 to 1. Fig. 25 shows the impact of parameter ξ on PDR for both narrow and wide FoV when $T = 1.5$s. A careful inspection of both Fig. 25 and Fig. 21 (for $T = 1.5$s) reveal that normalization achieved a significant increase in performance in terms of PDR for narrow FoV scenarios. More specifically, there were increases in PDR of up to $12\%, 6\%$ and 7% for $25, 35$ and 45 pkts/sec respectively, when $\xi = 0.5$ or 0.75. The poor performance of wide FoV scenarios does not allow for accurate conclusions.

As shown in Fig. 25, especially for narrow FoV scenarios, low PDR was achieved as $\xi \to 0$ and $\xi \to 1$. At low ξ_l values, weak attraction was exercised by each idle node l, even if these nodes were able to accommodate incoming traffic load. Since idle nodes are usually found at the borders of the packet flock, low ξ values 'force' packet flocks move in a coherent formation. In this case, a number of available paths were left unexploited while other (popular paths) faced overloading, thus resulting in low PDR. On the other hand, at high ξ_l values, each idle node l was exercising strong attraction (causing high packet spreading towards the border of the flock). In this case, 2 problems may occur: (a) There is no evidence of the channel quality in the vicinity of each idle node, thus high number of losses are expected to arise if the channel is busy. (b) Large number of packets are attracted to the borders of the flock (left and right), where the majority of idle nodes are. At the same time, packets are also attracted to the sink due to the inherent attraction of the magnetic field. Thus, packets 'flying' at the borders

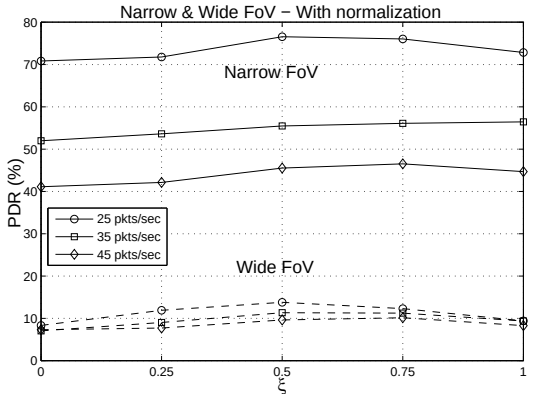

Fig. 25. Flock-CC v.2.2, step 2 (normalization of repulsion and attraction forces): Packet delivery ratio (PDR) for narrow and wide FoV, when $T = 1.5$s.

of the flock collide with ongoing packets 'flying' through the center of the flock, resulting in low PDR. Fig. 25 suggests that a good compromise value for ξ can be either 0.5 or 0.75. These values also resulted in low EED as shown in Fig. 26.

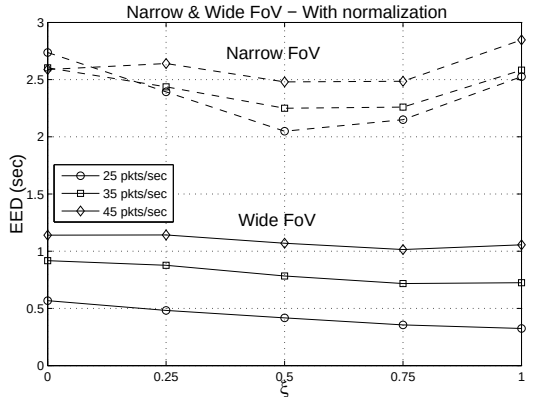

Fig. 26. Flock-CC v.2.2, step 2 (normalization of repulsion and attraction forces): End to end delay (EED) for narrow and wide FoV, when $T = 1.5$s.

Despite the improvement of performance, normalization did not tackle the problem of packet loops (mentioned in step 1).

Step 3**:** In this step, the attractiveness to packets (and hosting nodes) in the FoV was differentiated on the basis of different hop distances. The existence of nodes with different hop distances in the FoV was feasible when wide FoV was used.

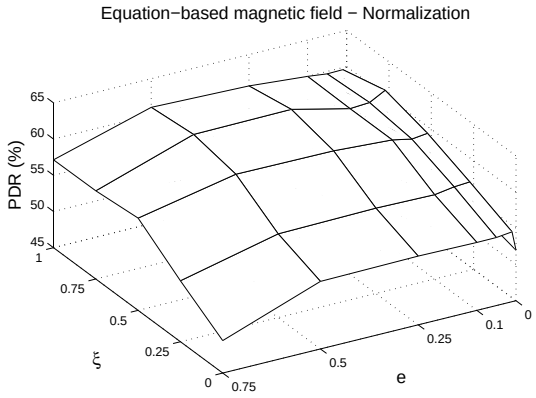

Fig. 27. Flock-CC v.2.2, step 3 (equation-based differentiated attractiveness): Packet delivery ratio (PDR) for narrow ($e = 0$) and wide FoV, for 35 pkts/s and $T = 1.5$s.

In the equation-based attractiveness variation strategy, the parameters e and ξ were chosen to range from 0 to 1. When $e > 0$, packets were allowed to move to nodes with either shorter or equal hop distance. This is interpreted as nodes were

perceiving wide FoV. On the other hand, when $e = 0$ packets could move only forward, thus the wide FoV degenerated into narrow FoV.

Fig. 27 illustrates the impact of e and ξ on PDR for 35 pkts/sec and $T = 1.5$s. It can be seen that for $e = 0$ (narrow FoV), results were similar to Fig. 25 (for 35 pkts/s), having PDR reaching its highest value of 57% at $\xi = 1$, i.e. when exploiting inactive nodes placed closer to the sink. The most remarkable observation, though, was the steep increase in PDR for the wide FoV, from 12% (without differentiated attractiveness, $\xi = 0.5$, see Fig. 25) to 62% (with differentiated attractiveness, $e = (0.25, 0.5)$ and $\xi = (0.75, 1)$, see Fig. 27). The reason is that nodes at equal hop distance were assigned an adequate attractiveness (parameter e), while idle nodes were highly attractive. Thus, packets could choose alternative paths to the sink involving non overloaded nodes without being trapped in loops (this happens when nodes at equal hop distance are highly attractive, $e = (0.75, 1)$). The same observations applied for traffic rates of 25 and 45 pkts/s.

The combination of the wide FoV and the differentiated attractiveness exploits the availability of many alternative paths to the sink (wide FoV characteristic) as well as involves stronger attraction to nodes closer to the sink (narrow FoV characteristic).

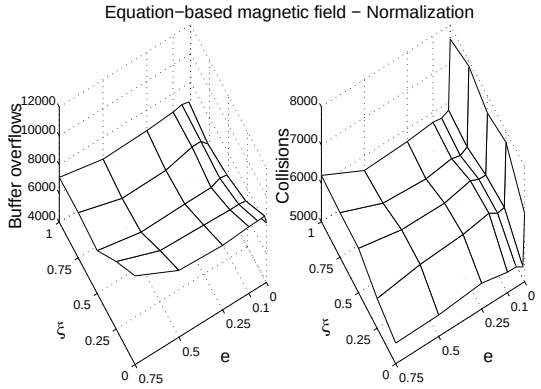

Fig. 28. Flock-CC v.2.2, step 3 (equation-based differentiated attractiveness): Packet loss for narrow ($e = 0$) and wide FoV, for 35 pkts/s and $T = 1.5$s.

As shown in Fig. 28, the existence of many alternative paths to the sink, including nodes placed at equal hop distance ($e > 0$), led to the decrease in the number of wireless channel collisions compared to narrow FoV scenarios ($e = 0$). The smallest number of collisions was achieved when $e = (0.25, 0.5)$ and $\xi = (0.75, 1)$. The highest number of collisions occurred for $e = 0$, regardless of ξ value. In this case, packets were 'forced' to move only forward, something that led to routing problems when front nodes were considered unreachable[5]. In the case of unreachable front nodes, packets were trapped in the network. After a given number of retransmission attempts causing high number of collisions, packets were dropped. High number of collisions was also observed for $e = 0.75$ and $\xi \geq 0.5$ since packets were trapped in loops.

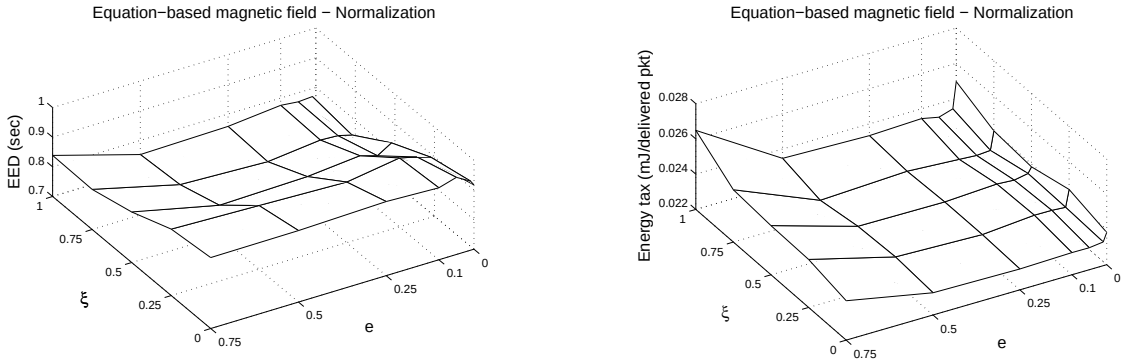

(a) End to end delay (EED)

(b) Energy tax

Fig. 29. Flock-CC v.2.2, step 3 (equation-based differentiated attractiveness): Narrow ($e = 0$) and wide FoV, for 35 pkts/s and $T = 1.5$s.

Fig. 28 shows that high number of buffer overflows was observed for $e = 0.75$ and $\xi = (0, 0.25)$. Even though a wide FoV was assumed (with high attraction to nodes at equal hop distance), packets could not exploit idle nodes (low ξ value) but

[5]A neighboring node is considered unreachable when the time elapsed from its last control message exceeds T_{lost}

they were 'forced' to move forward. On the other hand, low number of buffer overflows was perceived for $e = 0$ because low number of packets was arriving at the queues due to high collision rate.

Figs. 27 and 28 reveal that the highest PDR was achieved for $e = (0.25, 0.5)$ and $\xi = (0.75, 1)$ due to the low cumulative packet loss (collisions and buffer overflows). The same combination of values achieved the lowest EED as shown in Fig. 29(a) as well as the lowest energy tax spent per delivered packet as shown in Fig. 29(b).

The differentiated attractiveness proposed in Step 3 achieved better performance in terms of PDR, packet loss, EED and energy tax compared to previous approaches. The most remarkable observation was that the use of the wide FoV exploits the capabilities of the Flock-CC model and improves the offered quality. Thus, only the wide FoV was considered in the rule-based attractiveness variation strategy.

The rule-based attractiveness variation strategy simplifies the Flock-CC model by excluding parameter e. The only model parameter involved in the rule-based strategy was $0 \leq \xi \leq 1$. The Flock-CC approach was evaluated for all scenarios of Fig. 13, having $T = (0.5, 1, 1.5, 2.0)$s and transmission rates of $25, 35$ and 45 pkts/s.

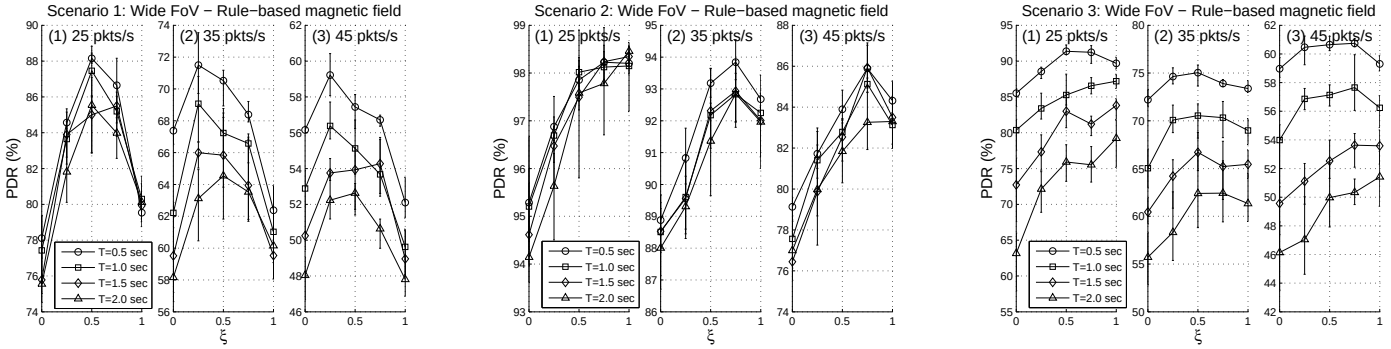

(a) Scenario 1 (b) Scenario 2 (c) Scenario 3

Fig. 30. Flock-CC v.2.2, step 3 (equation-based differentiated attractiveness): Packet delivery ratio (PDR) for wide FoV.

Fig. 30 illustrates the PDR for all three scenarios. The first important observation is that the rule-based strategy experienced improved performance compared to the equation-based strategy. More specifically, as shown in Fig. 30(a)(2) involving scenario 1, the mean PDR for the rule-based approach reached 66% (for 35 pkts/s, $T = 1.5$s and $\xi = 0.25$), while the highest PDR value for the equation-based strategy was 60% as shown in Fig. 27.

A quick inspection of the results reveal that the setting $T = 0.5$s achieved consistent, outstanding behavior across almost all scenarios of different T values. This observation was rather expected since frequent updates keep the flock always informed about network state. This of course happens at the cost of high energy expenditure as shown later, in Fig. 35. In addition, results showed that in scenario 1, high PDR was achieved when the parameter ξ was set between 0.25 and 0.75 (bell-shaped behavior). In scenario 2, PDR followed rising trends with the increase of ξ (a small decrease at $\xi = 1$ for medium and high data rates). In scenario 3, PDR exhibited bell-shaped behavior for $T = 0.5$s and 1s, whereas rising trends for $T = 1.5$s and 2s. Therefore, a good compromise value for all scenarios and traffic rates is $\xi = 0.5$. This setting allows some packets move through idle nodes (possibly placed at the borders of a flock) without provoking drainage of their resources.

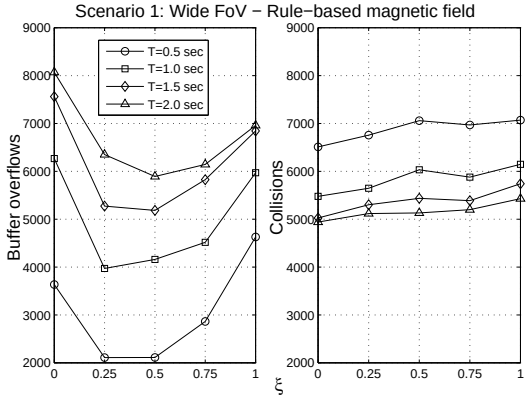

Fig. 31. Flock-CC v.2.2, step 3 (equation-based differentiated attractiveness): Packet loss for wide FoV, for the first scenario of operation, 35 pkts/s.

Packet loss is the other side of the coin of PDR. Fig. 31 discriminates the causes of packet loss in the first scenario (when 35 pkts/s). Results show that buffer overflows played a dominant role in the changes of PDR values since collisions did not

face large changes. More specifically, the number of buffer overflows depends heavily on the values of both ξ and T. Buffer overflows exhibited a reverse bell-shaped behavior with minimum at $\xi = (0.25, 0.5)$ and $T = 0.5$s for the reasons explained in the previous paragraph and below Fig. 22. On the other hand, collisions followed slightly rising trends with the increase in ξ and T.

Both the first and the third scenario involve the same set of active nodes, whereas only in the third scenario a high number of failing nodes provoked an undesirable situation. However, under certain conditions the third scenario outperformed (in terms of PDR) the first scenario. A closer look on Figs. 30(a) and 30(c) reveals that for $T \leq 1$s the third scenario achieved higher PDR than the (failure-free) first scenario (in all traffic rates). In low T values ($T \leq 1$s) where control packets were broadcasted quite frequent, the Flock-CC mechanism was kept updated regarding the network state. Thus, in the third scenario packet flocks recovered quickly from problems caused by node failures and managed to bypass the obstacle of dead nodes choosing alternative, but less congested paths to the sink. As shown in Fig. 32(b), these paths were not adjacent, thus minimizing the number of packets lost due to collisions.

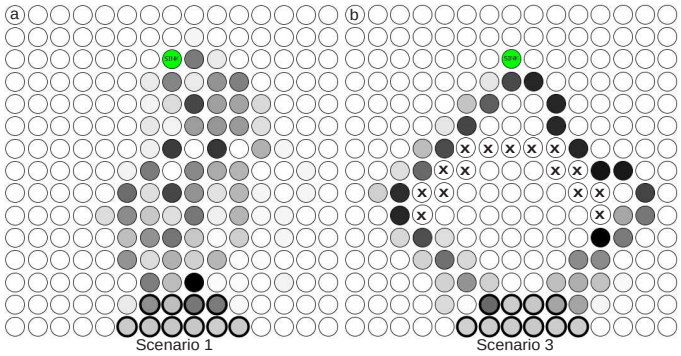

Fig. 32. Flock-CC v.2.2, step 3 (equation-based differentiated attractiveness) - Network snapshot: (a) scenario 1, (b) scenario 3). Color intensity indicates the intensity of packets visiting each node within a 1-second time slot.

On the other hand, in the first scenario, packet flocks followed a number of shortest, but adjacent, paths to the sink (see Fig. 32(a)). This movement of packets caused high number of collisions compared to the third approach. Fig. 33 shows that the number of packets lost due to collisions in the third scenario were remarkably less (especially for $T = 0.5$s and $T = 1$s) than the corresponding experiments of Fig. 31. As a result, the cumulative number of packets lost was smaller in the third scenario. When $T > 1$s the cumulative number of packets lost in the third scenario exceeded the corresponding cumulative losses of the first scenario. The problem was attributed to the unresponsiveness of the Flock-CC approach to network changes (failing nodes) resulting in the increase of buffer overflows close to the dead zone.

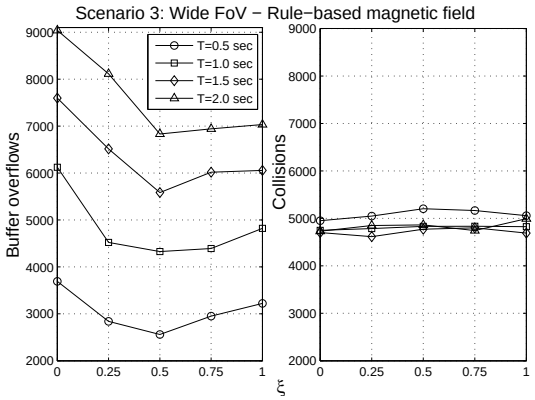

Fig. 33. Flock-CC v.2.2, step 3 (equation-based differentiated attractiveness): Packet loss for wide FoV for the third scenario of operation, 35 pkts/s.

As far as the end-to-end delay is concerned, Fig. 34 shows that in the first scenario low end-to-end delays (i.e. fast transitions of packets to the sink) were observed for $\xi = (0.25, 0.5, 0.75)$. The same observation applied for the 2 other scenarios.

Fig. 35 shows that energy expenditure exhibited similar increasing trends to the number of collisions as ξ was approaching 1. This is attributed to the intensity of packet spreading (towards idle nodes at the borders of the flock) which was getting stronger with the increase of ξ.

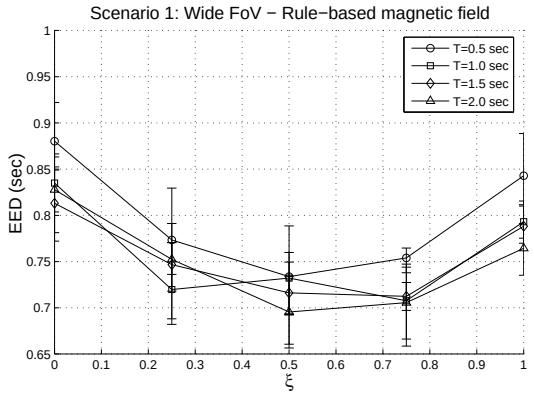

Fig. 34. Flock-CC v.2.2, step 3 (equation-based differentiated attractiveness): End to end delay (EED) for wide FoV for the first scenario of operation, 35 pkts/s and $T = 1.5$s.

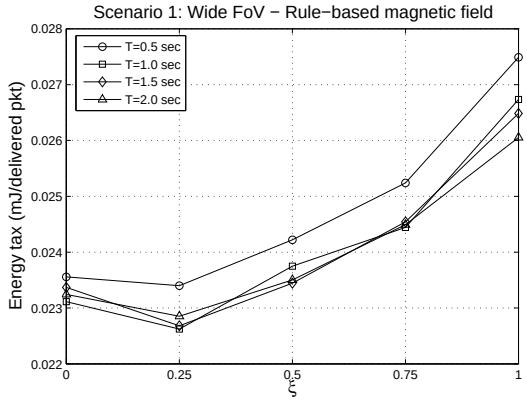

Fig. 35. Flock-CC v.2.2, step 3 (equation-based differentiated attractiveness): Energy tax for wide FoV for the first scenario of operation, 35 pkts/s and $T = 1.5$s.

4) Flock-CC v.2.3: In the third stage, Flock-CC v.2.3, perturbation was involved in the model. Two random selection techniques were used: roulette wheel selection and rank selection. Fig. 36 illustrates the PDR for the rank-based selection strategy for all three scenarios of Fig. 13 with respect to parameters T and ξ, when nodes were sending at 35 pkts/s. The results were compared to the corresponding scenarios without randomness, choosing the value of ξ that exhibited the best behavior (scenario 1: $\xi = 0.25$, scenario 2 : $\xi = 0.75$, scenario 3: $\xi = 0.5$).

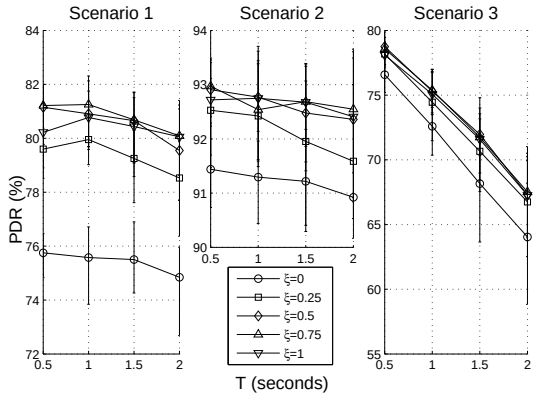

Fig. 36. Flock-CC v.2.3, rank-based selection: Packet delivery ratio (PDR) for 35 pkts/s.

In the first scenario, PDR reached 82% for $T = 1$s and $\xi = (0.5, 0.75)$ demonstrating an increase of 10% compared to the second approach (rule-based strategy without randomization) for $T = 0.5$s and $\xi = 0.25$. Poor performance was observed for $\xi = (0, 0.25)$. An interesting observation is that PDR did not deteriorate heavily with the increase of T from 0.5s to 2s

as happened in all the previous approaches. The feature of exploration that emerges from the randomized selection of new hosting nodes allows for traffic distribution through alternative paths to the sink even when information about network state and desirability evaluations are infrequently updated. In the second scenario, randomization did not improve PDR any further than what achieved in the second approach. Also the value of T did not seem to influence the offered quality, but this was also perceived in all approaches. The reason for these two observations is because the problem of congestion was less intensive in the second scenario. In the third scenario, random selection was found to be effective exhibiting an increase of 4% against the second scenario for $T = 0.5$s (up to 10% increase for $T = 2$s). The highest PDR was observed for $T = 0.5$s (regardless of ξ value) since the existence of node failures necessitated frequent updates (as happened in all previous approaches for scenario 3). The same observations applied for higher traffic rates (e.g. 45 pkts/s) as shown in Fig. 37.

Based on the results of Figs. 36 and 37, a good compromise parameter setting for all scenarios is $\xi = 0.5$ or $\xi = 0.75$ and $T = 0.5$s. However, to avoid high energy expenditure parameter T can be set to 1s. Alternatively, an adaptive mechanism can be used to variate the value of T according to the changes in network state. Of course, this can be done at the cost of adding extra complexity on each node.

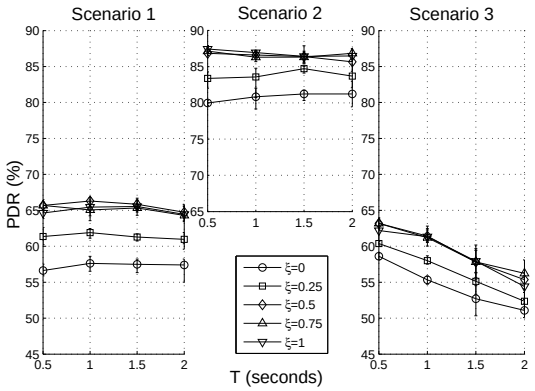

Fig. 37. Flock-CC v.2.3, rank-based selection: Packet delivery ratio (PDR) for 45 pkts/s.

Fig. 38 depicts the PDR for the roulette wheel-based selection strategy for all three scenarios, when 35 pkts/s. It can be seen that the results followed the same trends as in rank selection. However, the values of PDR were $1 - 3\%$ lower in roulette wheel selection.

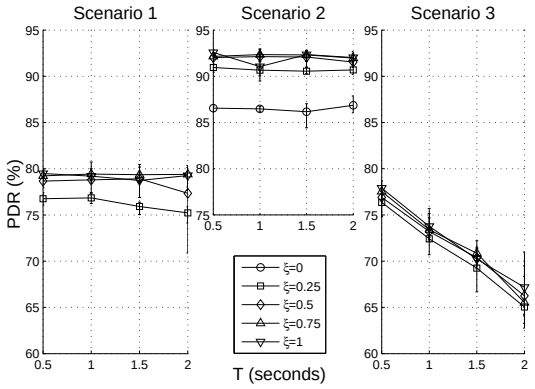

Fig. 38. Flock-CC v.2.3, roulette-based selection: Packet delivery ratio (PDR) for 35 pkts/s.

Fig. 39 discriminates the causes of packet loss in the first scenario (35 pkts/s) for both selection strategies. Rank selection was shown to outperform roulette wheel selection exhibiting lower number of buffer overflows than roulette wheel selection for almost every value of T and ξ. It is worth noting that the number of buffer overflows was remarkably increased for $\xi = (0, 0.25)$ for both selection strategies, whereas the number of collisions was very low for the same values. The lowest number of packets lost was achieved under the rank selection strategy, for $T = 0.5$s and $\xi = 0.75$.

As shown in Fig. 40, the rank selection strategy achieved remarkably lower EED (≈ 335ms in the best case, for $\xi = 0.75$) compared to the roulette wheel strategy (≈ 435ms in the best case). This observation is in line with the number of packet losses in each strategy. The low number of losses observed in the rank selection strategy is interpreted as having less number

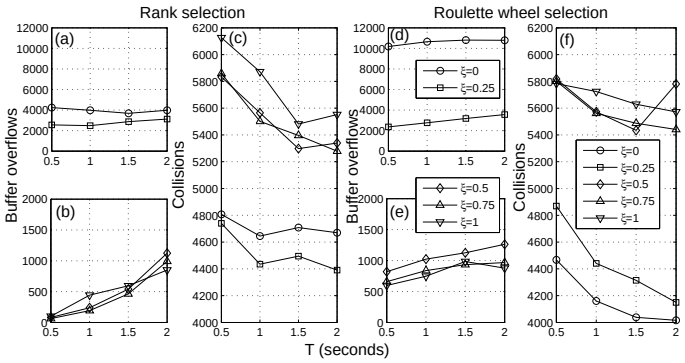

Fig. 39. Flock-CC v.2.3: Packet loss, first scenario, for 35 pkts/s: (a)-(c) rank selection, (d)-(f) roulette wheel selection.

of retransmissions, and thus faster transitions of packets to the sink. EED is evaluated on the basis of packets successfully delivered at the sink. Thus, results for $\xi = (0, 0.25)$ were omitted due to the high number of losses.

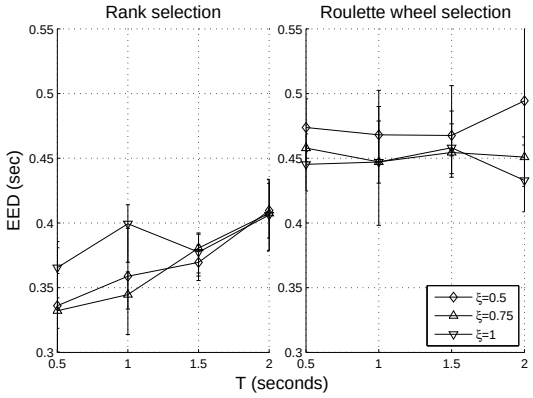

Fig. 40. Flock-CC v.2.3: End to end delay (EED) for 35 pkts/s: (a) rank selection, (b) roulette wheel selection.

Fig. 41 reveals that both approaches paid almost the same energy tax for the first scenario. Results confirmed the intuitive reasoning that low T values lead to high energy tax.

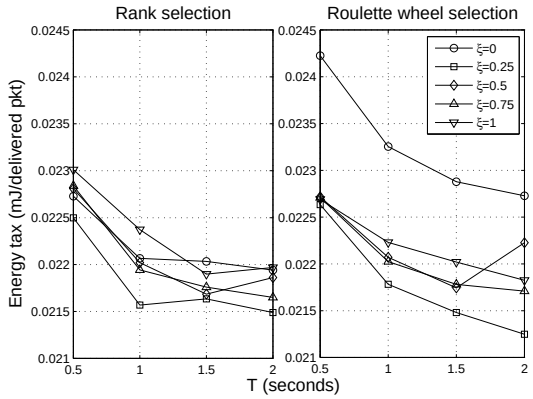

Fig. 41. Flock-CC v.2.3: Energy tax, first scenario, for 35 pkts/s: (a) rank selection, (b) roulette wheel selection.

Taking all the results of this section into consideration it is apparent that each characteristic of natural bird flocks is a quite necessary building block for developing an effective and efficient flock-based congestion control approach. The third stage, Flock-CC v.2.3, with rank selection strategy (incorporating all flocking characteristics) was shown to outperform the previous approaches in all scenarios and consists the final stage of the Flock-CC model development. A good compromise value for the single parameter used in this approach, ξ, was 0.75.

C. Emergent behavior of group-level transitions

This section evaluates the emergent behavior of the collective motion of packet flocks through the network under changing conditions. Flock-CC v.1 and Flock-CC v.2.3 were considered using the lattice topologies of Figs. 12 and 13, where the sink node is depicted in the upper side of each figure. Flock-CC v.1 was also tested in the random topology. In all figures, active nodes are highlighted by bold circles.

Flock-CC v.1 The self-adaptive nature of the first model was tested using scenarios 2 and 4.

The *emergent flocking behavior* of the collective packets movement through the lattice network is indirectly illustrated in Fig. 42 on the basis of the total number of packets arrived at each node. The darker the color of a node, the lower the number of packets visited that node, while unvisited nodes remain white. The values of α, e, c and T were set to $0.4, 0.6, 0.5$ and 1.0s respectively.

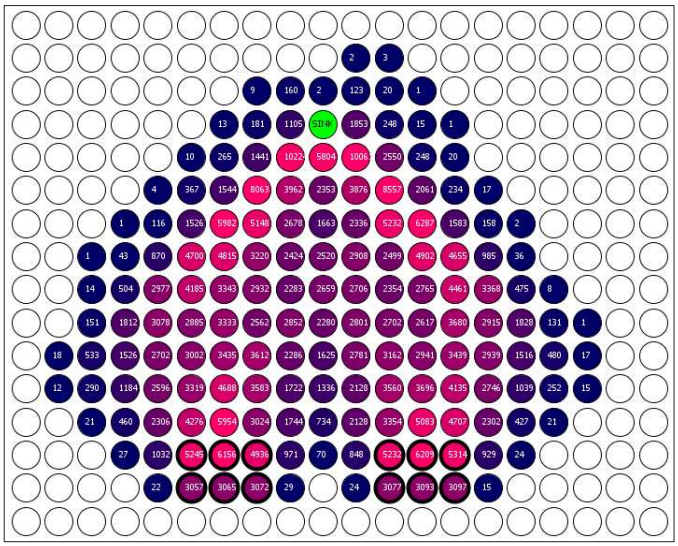

Fig. 42. Flock-CC v.1 Emergent flocking behavior: Total number of packets arrived at each node (throughout the simulation scenario 3) for the transmission rate of 35pkts/sec for $\alpha = 0.4, e = 0.6, c = 0.5$.

Fig. 42 shows that the behavior of moving packets successfully mimicked the obstacle avoidance behavior of bird flocks. These results highlight the *self-adaptiveness* of the Flock-CC mechanism to changing network and traffic conditions. In addition, it was shown that packets were moving apart to avoid congestion phenomena, thus causing traffic spreading among available paths to the sink. Therefore, the network energy expenditure is expected to be 'fairly' shared among these nodes, resulting in increased network lifetime. Increased packet concentration was observed on nodes located close to the sink due to the converging nature of the traffic.

The emergent behavior of the collective motion of packet flocks in a random topology is investigated below. The sink node is depicted in the middle of Fig. 43 (pointed out by a black arrow), while active nodes are highlighted by bold circles in the upper right corner of the network. The values of α, e, c and T were set to $0.5, 0.5, 0.25$ and 1 s respectively.

As can be seen, due to the flocking behavior, packets were spread in the network exploiting all available paths whilst moving towards the sink. There were two shortest paths to the sink (indicated by the two arrows in Fig. 43) which were traversed by the majority of the packets. Furthermore, the rest of the packets, which were repelled by packets located on the highly crowded nodes (as dictated by the bird flocking behavior), followed alternative paths (dark shaded nodes).

Flock-CC v.2.3 The *emergent flocking behavior* of the collective packets movement in Flock-CC v.2.3 is indirectly illustrated in Fig. 44 on the basis of the total number of packets arrived at each node. Scenarios 2 and 3 were taken into account. The values of τ and T were set to 0.75 and 0.5 respectively in both scenarios.

The emergent behavior can be perceived: (a) directly by the visual representation of flock movements and (b) indirectly on the basis of the performance evaluation metrics.

Evaluation results based on scenario 2 (and transmission rate of 35 pkts/s) demonstrated the obstacle avoidance behavior of packet flocks. Fig. 44(a) depicts the bird-like motion of packets generated by the front set of the 5 dark grey shaded nodes. As can be seen, due to the flocking behavior, packets were spread in the network choosing numerous of paths to the sink. Fig. 44(b) shows that after the initiation of the back set of nodes, the new flock of packets split apart into two separate groups in order to avoid colliding with packets generated by the front set of nodes. The direction of motion of the two sub-flocks is highlighted by transparent arrows. When the front set of node stopped transmitting, the two sub-flocks rejoined to a single flock moving over the area that used to be a congestion region.

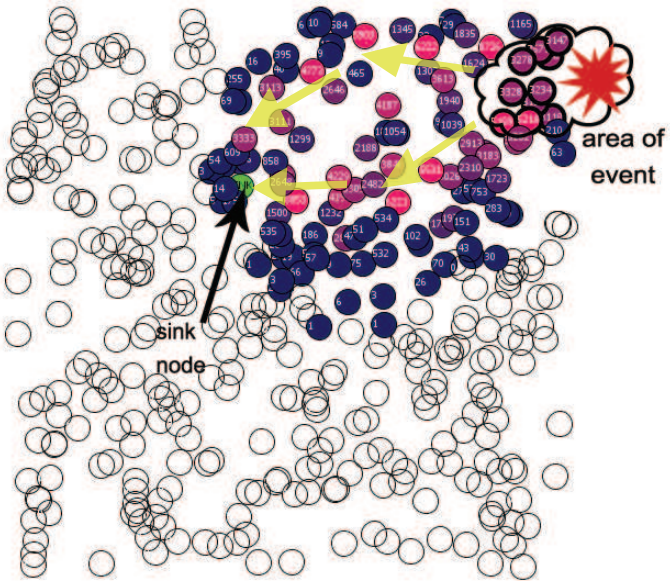

Fig. 43. Flock-CC v.1 Emergent flocking behavior: Total number of packets arrived at each node (throughout the simulation scenario 4) for the transmission rate of 35pkts/sec for $\alpha = 0.5, e = 0.5, c = 0.25$.

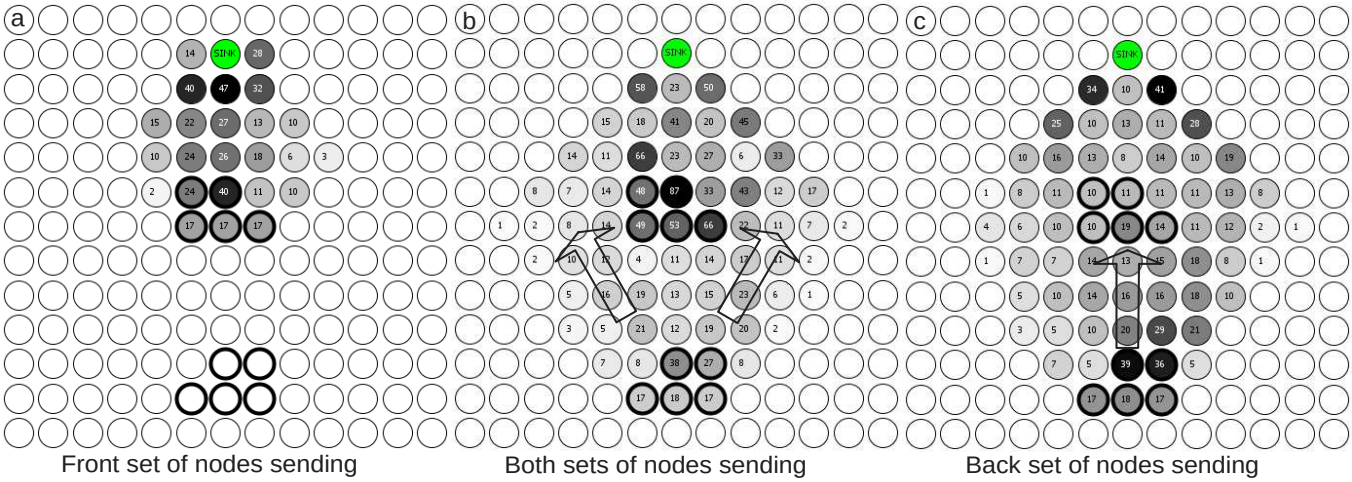

Fig. 44. Flock-CC v.2.3 Emergent behavior: Visual representation of moving packets in scenario 2 (35 pkts/s). The number of packets visiting each node within a 1-second time slot is indicated inside every node.

Fig. 45 shows the emergent behavior of moving packets before and after node failures in scenario 3. The emerging reorganization of moving packets after node failures is shown in Fig. 45(b), where the single flock of packets split into two smaller compact groups, both of which 'flew' around the 'dead' zone.

This section focused on the ability of moving packets to mimic the obstacle avoidance behavior of bird flocks. Visual representations demonstrated the *self-adaptiveness* of the proposed approach to changing traffic (Fig. 44) and network conditions (Fig. 45). In particular, it was shown that packets were moving apart to avoid queue and channel loading phenomena or node failures, thus causing traffic spreading among available paths to the sink. Therefore, the network energy expenditure was 'fairly' shared among nodes along these paths, resulting in increased network lifetime. If packets were routed via a single path, or were spread among multiple paths in an unbalanced manner, some of these paths could progressively become over-utilized, causing unbalanced network energy expenditure.

The emergent behavior was also perceived through performance evaluation metrics. The previous section presented a bottom-up approach of developing a flock-based congestion control protocol of increasing sophistication and similarity to natural bird flocks. Fig. 46 compares the PDR obtained by running scenario 1 at 35 pkts/s with 3 congestion control models of increasing sophistication. These 3 models were extracted from the 3 approaches of the previous section. The first model refers to the third approach (with the rank selection strategy) involving all flocking characteristics. The second model refers to the second approach (with the rule-based strategy) that excluded randomization. Finally, the third model is loosely related to the second

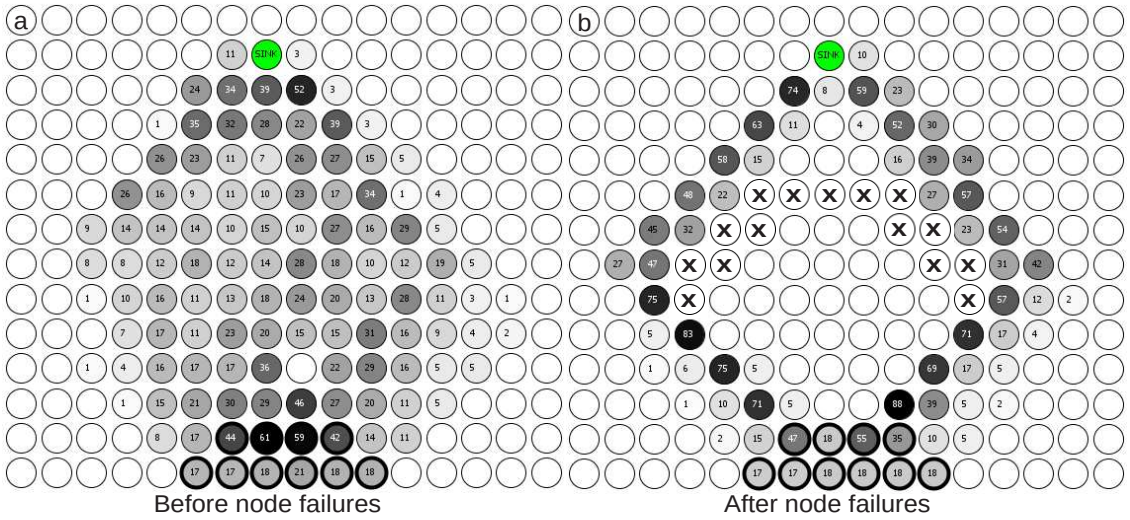

Fig. 45. Flock-CC v.2.3 Emergent behavior: Visual representation of moving packets in the presence of failing nodes in scenario 3 (35 pkts/s).

approach involving the FoV and the magnetic field but without taking into account local interactions and randomization. The first approach (without FoV and magnetic field) was not considered due to its poor performance.

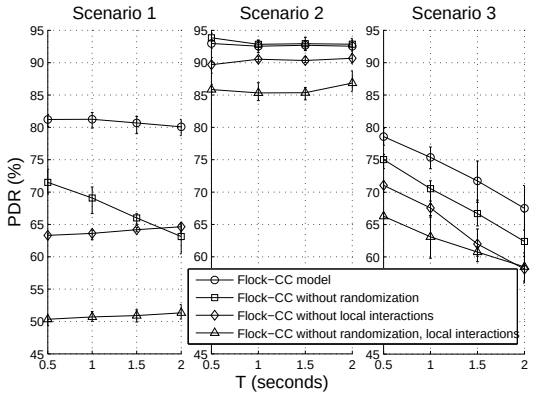

Fig. 46. Flock-CC v.2.3 Emergent behavior: The effect on packet delivery ratio (PDR).

As can be seen, the highest PDR (with the smallest deviation from mean value) was achieved when all flocking characteristics were incorporated in the congestion control model, especially for the scenarios 1 and 3. The contribution of perturbation (for $T = 0.5$s) in scenario 1 was $\approx 10\%$ (the difference between the first and the second model), whereas in scenario 3 was $\approx 5\%$. In scenario 2, where light congestion phenomena occurred, there was no significant contribution of perturbation. Increasingly, the contribution of the local interactions in scenario 1 was $\approx 15\%$ (the difference between the second and the third model), in scenario 2 was $\approx 4\%$, whereas in scenario 3 was $\approx 8\%$. Similar behavior was observed for end-to-end delay evaluations as shown in Fig. 47.

D. Robustness in failure prone environments

Sensor nodes are prone to failures, mainly due to fabrication process problems, environmental factors (disasters), enemy attacks, and battery power depletion. Both Flock-CC v.1 and Flock-CC v.2.3 exhibit robustness against node failures due to the inherent tendency of individuals to follow other flockmates that manoeuvre to avoid obstacles such as failing nodes.

Flock-CC v.1 The self-adaptive nature of the first model was tested using the scenarios 3 and 4.

It is expected that the self-adaptive nature of the flock-based models will enhance robustness against failing nodes. As far as the first model is concerned, the bird-like motion of packets generated by the heavy grey shaded nodes in the middle bottom part of Fig. 12 (scenario 3) before node failures is similar to Fig. 42.

Evaluation results based on scenario 3 (and transmission rate of 35 pkts/sec) present the obstacle avoidance behavior of packet flocks when nodes located in the heavy grey shaded zone failed (at $t = 60$). Figs. 48(a) and (b) show the emerging

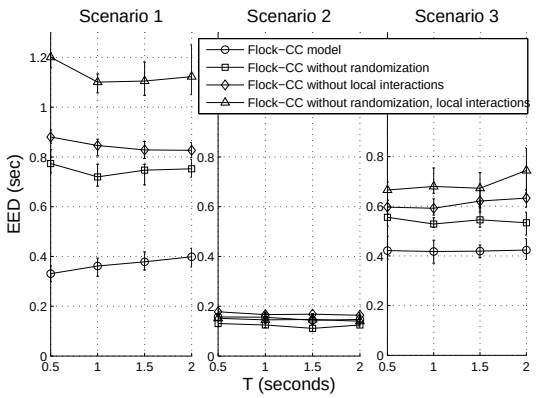

Fig. 47. Flock-CC v.2.3 Emergent behavior: The effect on end-to-end delay (EED).

flocking behavior of packets, whilst avoiding 11 failed nodes (marked with the letter 'X') located within the path to the sink. Fig. 48(a) illustrates a snapshot of the network state (instantaneous number of packets arrived at each node) right after node failures, at time $t = 65$ sec. As can be seen, the main packet flock began to split apart into two separate packet flocks in order to navigate around the dead zone. Fig. 48(b) shows that after a small period of time ($t = 83$ sec.) the two packet flocks created completely distinct paths to the sink.

Fig. 49 shows two network snapshots, before and after node failures in the random topology of scenario 4. It is apparent that the Flock-CC approach displayed outstanding flocking behavior in the presence of numerous node failures, and exemplified all of the characteristics of a bird flock in terms of obstacle avoidance and manoeuvring around the zone of dead nodes. Results showed that Flock-CC provided graceful performance degradation when node failures occurred exhibiting a slight decrease in packet delivery ratio and a small increase in end-to-end delay.

Flock-CC v.2.3 The third scenario was used to demonstrate the robust nature of Flock-CC v.2.3. Fig. 45 shows a couple of network snapshots before and after node failures. It is apparent that the Flock-CC approach displayed outstanding flocking behavior in the presence of numerous node failures, and exemplified all of the characteristics of a bird flock in terms of obstacle avoidance and manoeuvring around the zone of dead nodes.

E. Comparative studies

Both Flock-CC models (that incorporate both routing and congestion control capabilities) were compared with (a) a conventional congestion-free multi-path routing protocol based on shortest paths, (b) a typical congestion-aware routing protocol that routes packets over multiple paths, choosing each time the least congested node in terms of queue length, and (c) a well known single-path routing protocol for adhoc networks, AODV [22].

Flock-CC v.1: In Flock-CC v.1, both scenarios 1 and 4 were used in comparative evaluations. For scenario 1, the values of α, e and c were set to $0.4, 0.6$ and 0.5 respectively, which demonstrated the best performance.

Results (Fig. 50) showed that the proposed approach clearly outperformed all other approaches in terms of both PDR and EED, for all transmission rates. From the perspective of PDR, Fig. 50(a) shows that the Flock-CC v.1 delivered 18% more packets than the congestion-free protocol under low loads (25 pkts/sec), as well as 23% more packets under high loads (45 pkts /sec), where congestion phenomena were more intensive. Similarly, Flock-CC v.1 achieved $12 - 15\%$ higher PDR compared with the congestion-aware routing protocol. These results show that when there are multiple shortest paths to the sink, Flock-CC v.1 allowed packets to exploit available resources on nodes involved in these paths (traffic spreading). The other two protocols (congestion-free, congestion-aware) did not allow for packet spreading among all available paths, resulting in over-utilization of some paths. In the congestion-free protocol, packets were sent over the shortest path, while the congestion-aware routing protocol could allow for packet spreading if queues were filling up. In line with the previous statement, Fig. 50(b) shows that the proposed approach exhibited the lowest EED among the other protocols for every transmission rate, because traffic spreading prevented augmented buffer occupancies, and thus larger queueing delays, which were observed in the other two scenarios. In all scenarios described earlier the proposed approach outperformed over the other two approaches.

For scenario 4 (random topology), parameters α, e and c were set to $0.5, 0.5$ and 0.25 respectively. Fig. 51 shows that Flock-CC v.1 approach clearly outperformed all other approaches in terms of both PDR and EED, for all transmission rates.

From the perspective of PDR, Flock-CC v.1 delivered around 16% more packets than the congestion-free protocol under low and medium loads, and around 10% more packets under high loads. Similarly, Flock-CC v.1 achieved $5 - 7\%$ higher PDR compared with the congestion-aware routing protocol. Flock-CC v.1 also outperformed AODV by $38 - 60\%$.

For the congestion-free protocol, packets were sent over the shortest path, while the congestion-aware protocol allows for packet spreading if queues were filling up. This behavior is illustrated in Figs. 51(c) and (d). A remarkable observation is

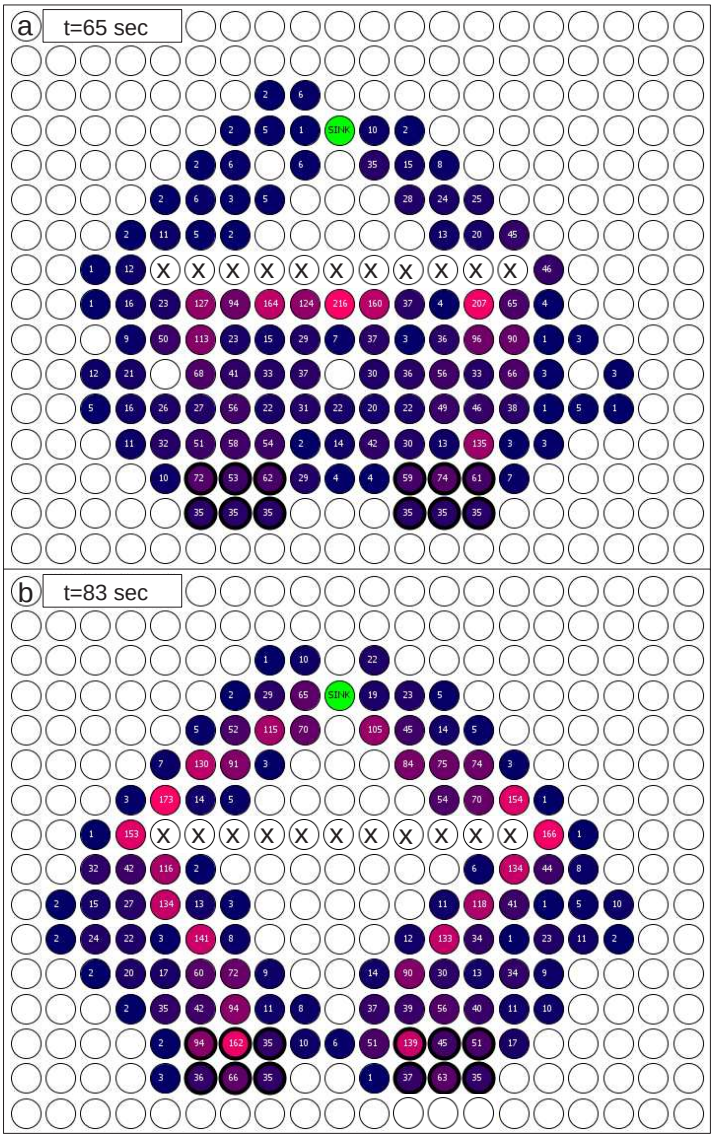

Fig. 48. Flock-CC v.1: Failing nodes (nodes fail at $t = 60$ secs): Instantaneous number of packets arrived at each node for the transmission rate of 35pkts/sec at: (a) $t = 65$, and (b) $t = 83$.

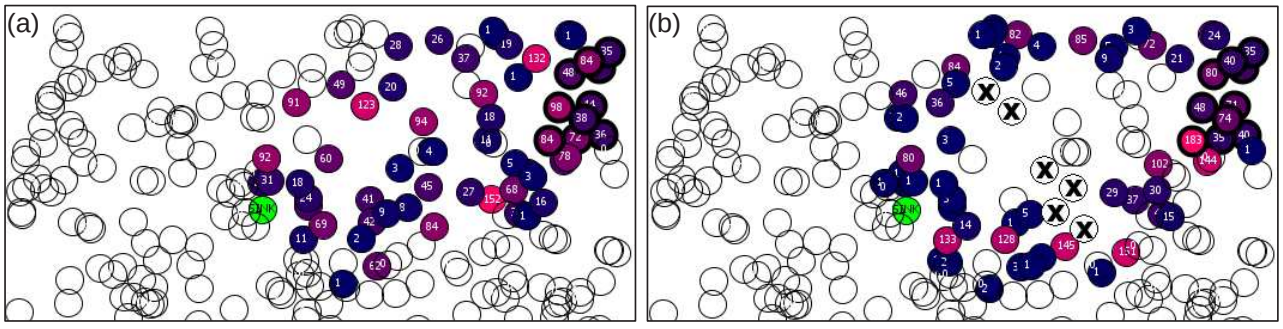

Fig. 49. Flock-CC v.1: Emergent behavior of moving packets at the presence of failures: (a) Before failures, (b) After failures. A small region of the network involving packet activity is illustrated.

that Flock-CC v.1 exhibited low buffer overflows compared to the congestion-free and congestion-aware protocols due to its traffic spreading ability. AODV achieved minimal buffer overflows something that is explained by looking at Fig. 51(d). AODV suffered heavily from collisions, while the problem worsened with the increase of traffic load. This problem was attributed to

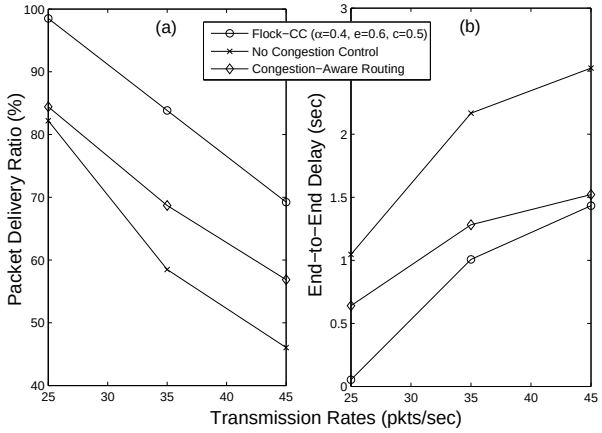

Fig. 50. Flock-CC v.1: Comparative experiments for scenario 1.

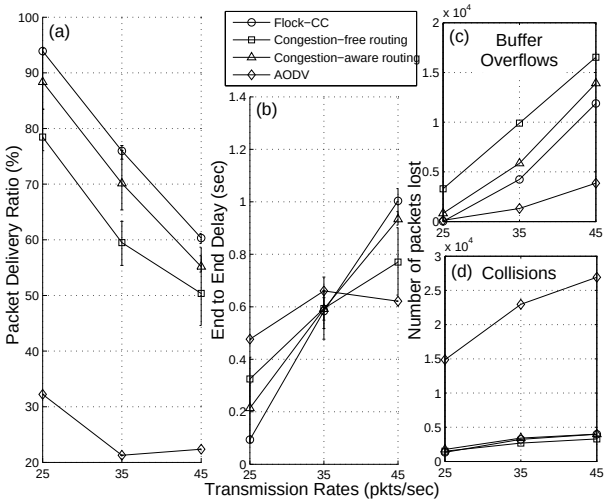

Fig. 51. Comparative experiments.

the high number of broadcasted control messages that led to wireless channel capacity saturation. As a result, buffers were rarely filled up. The other three protocols exhibited significantly lower number of collisions.

Fig. 51(b) shows that Flock-CC v.1 exhibited the lowest EED among the other protocols for every transmission rate, because traffic spreading prevented augmented buffer occupancies which contribute to larger queueing delays. Note that only packets successfully received at the sink were involved in EED evaluation. In line with this statement, AODV exhibited low EED in high load conditions, since the majority of packets were lost.

Flock-CC v.2.3: Results of Fig. 52 show that Flock-CC v.2.3 clearly outperformed no congestion control and congestion aware routing protocols in terms of both PDR and EED, for all traffic loads and scenarios. The results for the AODV protocol were omitted due to the very low performance of the protocol compared to the other protocols shown in Fig. 52.

From the perspective of PDR, Fig. 52 shows that Flock-CC v.2.3 delivered around $15\%, 23\%$ and 19% more packets for scenario 1 than the no congestion control protocol under low, high and extreme traffic loads respectively. The difference in PDR between scenarios 2 and 3 was smaller. Similarly, in scenario 1, Flock-CC v.2.3 achieved 2% to 8% higher PDR (better performance in low loads with decreasing trends in extreme loads) compared to the congestion aware routing protocol. Differences of 2% to 4% in PDR between scenarios 2 and 3 were observed.

Based on the outcomes of the comparative study, it can be argued that the controlled traffic spreading that emerged from the flocking behavior of packets allowed packets to exploit available resources on nodes involved in multiple paths to the sink, resulting in higher performance. The no congestion control and congestion aware routing protocols did not allow for packet spreading among all available paths, resulting in over-utilization of some (popular) paths. Under the no congestion control protocol, packets were solely sent over the shortest path(s), while the congestion aware routing protocol allowed for packet spreading after the appearance of buffer overflows. This behavior led to a high number of packet losses due to buffer overflows. Further results showed that Flock-CC v.2.3 exhibited extremely low buffer overflows compared to both protocols due to the

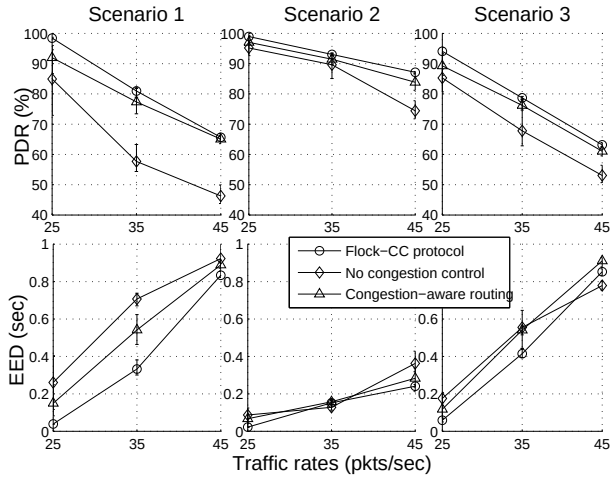

Fig. 52. Flock-CC v.2.3: Comparative experiments in scenarios $1-3$ for $T = 0.5$s. The performance of AODV was considerably poor, thus related results were omitted from this figure.

traffic spreading ability of the bird flocking behavior.

In addition, Fig. 52 shows that Flock-CC v.2.3 exhibited the lowest EED among the other protocols for every transmission rate and scenario, because traffic spreading prevented augmented buffer occupancies that contribute to larger queueing delays.

V. Conclusion and future work

This study focused on the bird flocking behavior to combat congestion in wireless sensor networks (WSNs). The synchronized group behavior of birds flocks and their ability to avoid obstacles is mimicked in order to control the motion of packet flocks through a network of constrained sensor nodes. Two Flock-CC models are proposed that guide packets towards the sink whilst avoiding congestion regions and dead node zones in a robust way. Increasingly, both proposed models contribute to the emergent behavior of high packet delivery ratio, low end-to-end delay and minimal energy tax.

The bio-swarm approach of Couzin [4] was reformulated from a metrical space to a topological space in order to manipulate the direction of motion of packets in WSNs influenced by local interactions among neighboring packets. In both proposed models, each packet perceives repulsive and attractive forces exhibited by other packets located on neighboring nodes within the field of view, and decides a new hosting node on the basis of a desirability function. The desirability of each potential next hop node is differentiated on the basis of magnetic field forces to account for biased selection of nodes located closer to the sink. Also, perturbation, which allows for exploration, is introduced to allow packets to pick random routes, and thus to avoid over-flooding popular (due to their low congestion levels) next hop nodes. The behavioral tendencies involved in the proposed models were simulated to study the effectiveness of the models in mimicking the collective behavior of bird flocks. Performance evaluations showed that the proposed models were able to alleviate congestion by balancing the offered load, while offering acceptable PDR especially in high load scenarios, fast delivery (small EEDs) of packets to the sink, and low energy tax. Furthermore, both Flock-CC models outperformed typical conventional congestion-aware and congestion-free routing approaches in terms of PDR in low, medium and high loads. The second model, Flock-CC v.2, is simpler than the first model, involving only one tunable parameter instead of three (hence easier to tune and thereafter deploy). Results showed that the final version of the second model, Flock-CC v.2.3, maintains comparably good performance characteristics compared to the first model, thus can be adopted.

Future work will investigate different functions for randomizing the attractiveness to the sink. Also, the performance in terms of power, as well as the inclusion of power in the desirability function remains a matter of further research. In addition, beyond the hop distance, new techniques for sink direction discovery are also left for future work. To conclude, an interesting idea is to investigate if and how the Flock-CC approach can operate in the presence of multiple sinks.

Acknowledgment

This work was supported in part by the GINSENG: Performance Control in Wireless Sensor Networks project funded by the 7^{th} Framework Programme under Grant No. ICT-224282 and the MiND2C: Mimicking Nature for Designing Robust Congestion Control Mechanisms in Self-Organized Autonomous Decentralized Networks project funded by the Research Promotion Foundation of Cyprus under Grant No. TPE/EPIKOI/0308(BE)/03.

REFERENCES

[1] P. Antoniou, A. Pitsillides, T. Blackwell, and A. Engelbrecht, "Employing the flocking behavior of birds for controlling congestion in autonomous decentralized networks," in *2009 IEEE Congress on Evolutionary Computation*, A. Tyrrell, Ed., IEEE Computational Intelligence Society. Trondheim, Norway: IEEE Press, 18-21 May 2009.

[2] P. Antoniou, A. Pitsillides, A. P. Engelbrecht, and T. Blackwell, "Mimicking the bird flocking behavior for controlling congestion in sensor networks (invited paper)," in *3rd International Symposium on Applied Sciences in Biomedical and Communication Technologies*. IEEE conference proceedings, November 2010.

[3] P. Antoniou, A. Pitsillides, A. P. Engelbrecht, T. Blackwell, and L. Michael, "Congestion control in wireless sensor networks based on the bird flocking behavior," in *4th IFIP TC 6 International Workshop on Self-Organizing Systems IWSOS*, ser. Lecture Notes in Computer Science, T. Spyropoulos and K. A. Hummel, Eds., vol. 5918. Springer, December 2009, pp. 220–225.

[4] I. D. Couzin, J. E. N. S. Krause, R. James, G. D. Ruxton, and N. R. Franks, "Collective memory and spatial sorting in animal groups," *Journal of Theoretical Biology*, vol. 218, no. 1, pp. 1–11, September 2002.

[5] I. F. Akyildiz, W. Su, Y. Sankarasubramaniam, and E. Cayirci, "Wireless sensor networks: a survey," *Computer Networks (Amsterdam, Netherlands: 1999)*, vol. 38, no. 4, pp. 393–422, March.

[6] E. Bonabeau, M. Dorigo, and G. Theraulaz, "Swarm intelligence: From natural to artificial systems," *J. Artificial Societies and Social Simulation*, vol. 4, no. 1, 2001.

[7] A. P. Engelbrecht, *Fundamentals of Computational Swarm Intelligence*. NJ: John Wiley & Sons, Jan. 2006.

[8] E. Bonabeau, M. Dorigo, and G. Theraulaz, "Inspiration for optimization from social insect behaviour," *Nature*, vol. 406, no. 2000, pp. 39–42, 2000.

[9] M. Dorigo and C. Blum, "Ant colony optimization theory: a survey," *Theor. Comput. Sci.*, vol. 344, no. 2-3, pp. 243–278, 2005.

[10] G. D. Caro, F. Ducatelle, and L. M. Gambardella, "Anthocnet: an adaptive nature-inspired algorithm for routing in mobile ad hoc networks," *European Transactions on Telecommunications*, vol. 16, no. 5, pp. 443–455, 2005.

[11] Z. Xiangquan, G. Lijia, G. Wei, and L. Renting, "A cross-layer design and ant-colony optimization based load-balancing routing protocol for ad-hoc networks," *Frontiers of Electrical and Electronic Engineering in China*, vol. 2, no. 2, pp. 219–229, April 2007.

[12] T.-F. Shih, "Particle swarm optimization algorithm for energy-efficient cluster-based sensor networks," *IEICE Trans. Fundam. Electron. Commun. Comput. Sci.*, vol. E89-A, no. 7, pp. 1950–1958, 2006.

[13] G. D. Caro, F. Ducatelle, and L. M. Gambardella, "Swarm intelligence for routing in mobile ad hoc networks," *Swarm Intelligence Symposium*, pp. 76–83, June 2005.

[14] C. W. Reynolds, "Flocks, herds and schools: A distributed behavioral model," in *SIGGRAPH '87: Proceedings of the 14th annual conference on Computer graphics and interactive techniques*. New York, NY, USA: ACM, 1987, pp. 25–34.

[15] W. Wiltschko, "Uber den einflu statischer magnetfelder auf die zugorientierung der rotkehlchen," *Z. Tierpsychol.*, vol. 25, pp. 537–558, 1968.

[16] A. Von Middendorf, "Die isepiptesen rublands," *Mem. Acad. Sci. St Petersbourg VI*, vol. 8, pp. 1–143, 1859.

[17] C. Viguier, "Le sens de lorientation et ses organes chez les animaux et chez l'homme," *Rev. phil. France Etranger*, vol. 14, pp. 1–36, 1882.

[18] W. Wiltschko and R. Wiltschko, "Magnetic orientation in birds," *The Journal of Experimental Biology*, vol. 199, pp. 29–38, 1996.

[19] D. Heyers, M. Manns, H. Luksch, O. Gunturkun, and H. Mouritsen.

[20]

[21] The Network Simulator NS-2, *http://www.isi.edu/nsnam/ns*. http://www.isi.edu/nsnam/ns/.

[22] C. E. Perkins, "Ad hoc on demand distance vector (aodv) routing," *RFC 3561*, 1997.